Sedimentation of a small sphere in stratified fluid

Hojun Lee,[1] Itzhak Fouxon,[1] and Changhoon Lee[1,2,*]
[1]*Department of Computational Science and Engineering, Yonsei University, Seoul 03722, Korea*
[2]*Department of Mechanical Engineering, Yonsei University, Seoul 03722, Korea*

(Received 30 November 2018; published 7 October 2019)

We report an extensive theoretical and numerical study of gravitational settling of small particles in a stratified fluid at rest. The particle motion creates a flow that advects the stratified agent, which in turn impacts the velocity by buoyancy. A peculiar insulation flow also exists when a particle and fluid at infinity are at rest, screening the particle from the outside gradients. We derive an integral representation for the linear coupled flow that holds at low Reynolds and Péclet numbers. The representation demonstrates that the far flow contains a previously unnoticed term that is produced by the thermal component of the fundamental solution. We obtain nontrivial symmetry relations that constitute a form of the Onsager reciprocal relations. Stratification is a singular perturbation: however small it is, far from the particle the flow is fast decaying and does not obey the slow power-law decay of the Stokes flow at zero stratification. We derive the enhancement of the drag force due to the stratification by adopting the integral equation on the surface traction. This allows one to find the force directly, circumventing finding the flow whose calculation demands the matched asymptotic expansions that complicated previous studies. In this way we are able to extend the domain of validity of the drag formula by orders of magnitude. We confirm the predictions by numerical simulations at low Reynolds numbers. We also performed simulations for a range of non-small Reynolds numbers where the flow is nonlinear, but the Reynolds number is not too large. The considered range of parameters demonstrates that inclusion of stratification might be necessary for correct prediction of the sedimentation velocity of plankton particles and small organic particles of marine snow. We provide the settling velocity of Volvox as an example. We sum up our observations by deriving an empirical fitting formula for the drag coefficient. Finally, we discuss the observability of the insulating flow around a floating body.

DOI: 10.1103/PhysRevFluids.4.104101

I. INTRODUCTION

Frequently, sedimentation of heavy particles in the atmosphere or the ocean occurs in the presence of stratification. The stratified regions where gradients of density hold (called pycnoclines in the aquatic context) are created by gradients of temperature or salinity. This makes the calculation of the settling velocity in the stratified fluid at rest a problem of great practical interest with a wide range of engineering and environmental applications. The relevance of this problem is not changed by the turbulence that is often present, despite the damping action of stratification. Indeed, for a linear friction law, turbulence does not change the mean settling velocity at all if the mean turbulent velocity in the particle frame is zero. This is readily seen by averaging the linear equation of motion. The effects of preferential concentration can produce an order-of-one change in the mean settling velocity [1]; however, a good starting approximation for the mean settling velocity in turbulence is

*clee@yonsei.ac.kr

still the settling velocity in the fluid at rest. The main application of the particle sizes considered in this work is to nonswimming plankton particles and organic particles of marine snow that are relevant in the oceanic carbon cycle; see, e.g., [2,3]. Besides practical applications, the problem also presents a significant theoretical challenge even in the limit of small particles, where linear equations apply. The flow is then described by a generalized bi-Helmholtz equation for which no analytical solution is available. The difficulty can be demonstrated by considering the fundamental solution, which is the flow driven by the point force; see List [4], Ardekani and Stocker [5], and also Zvirin and Chadwick [6]. Its Fourier transform can be obtained in elementary functions; however, the solution in real space cannot be written in closed form [4,5,7]. This implies that the more complex solution with the no-slip boundary condition on the surface of the moving particle cannot be obtained in closed form. Thus, the problem of finding the drag force on the particle sedimenting in the stratified fluid requires a study of limiting cases where the smallness of some parameter would allow the solution to be obtained. The most practical limit is that of weak stratification.

It could be thought that the impact of the stratification is small if the scale of density variations is many orders of magnitude larger than the size of the particle, because then the density is almost uniform on the scale of the particle. This is, however, not so because the scale L measuring the strength of the effects of stratification is due to the coupling of the velocity and density [8]. The parameters that enter this scale are similar to those in the Rayleigh-Bénard instability where instead of instability, a strong stabilizing effect holds at scale L. This scale, called below "the Rayleigh scale," is typically of the order of millimeters [8]. The motion of fluid masses at scales larger than L produces strong friction, described by the bi-Laplacian, and is damped [4,5,7,8]. Beyond the scale of order L, the fluid is effectively at rest. In fact, for the order-of-magnitude estimates, the effect of small stratification on particle translation in the fluid is similar to setting a rigid spherical wall of radius L. The smallness of stratification corresponds then to the limit of the distant wall. Thus, for a sphere with diameter d, the leading-order correction to the Stokes drag is of order d/L as in the classical Lorentz results for plane walls [9]. This order of the correction holds in the limit where the convection is negligible (low Reynolds and Péclet numbers), as was observed in [10]. These authors assumed $d/L \ll 1$ and considered matching of the nearly Stokes flow holding at scales r close to the particle, $r \ll L$, with the far flow at $r \gg d$ describable by the point force solution. In this work, we provide a simpler derivation without using the matched asymptotic expansions and series expansions of generalized functions of [10]. We also provide higher-order corrections in d/L, which significantly enlarges the range of parameters covered by the theory. In fact, the buoyancy enters the equations with the prefactor $(d/L)^4$ called below the Rayleigh number (it is the usual Rayleigh number used in the theory of convection with the particle diameter instead of the system size). This hints at the possibility of constructing a theory under the much less stringent condition $(d/L)^4 \ll 1$. In fact, the theory described in this paper works well until $d \sim L$. This has practical relevance. A millimeter-size particle that is slightly denser than water has a small Reynolds number. This particle is in the domain of validity of the theory (the Péclet number is small also). Its sedimentation velocity is changed by a factor of order 1 by stratification in comparison with the Stokes law estimate.

Previous theories used matched asymptotic expansions. The first treatment of the low-Reynolds-number case using this method was performed in the regime where the convection of the stratified agent is not small (finite Péclet number) [6]. Yick *et al.* [11] investigated the drag enhancement due to stratification experimentally and numerically, and observed incomplete agreement with [6]. The authors of [10], studying small Reynolds and Péclet numbers, besides deriving the d/L correction, considered the history force relevant for the time-dependent motions of the settling particle. It is very hard to see how their procedure can be extended to the case $(d/L)^4 \simeq 1$ where d can be comparable with L, invalidating the separation into inner and outer regions. In this work, we use the integral equation on the surface traction instead of using matched asymptotic analysis for the study of the force. This approach involves only the properties of the flow near the particle surface and does not need the far flow, which is nonperturbative. The equation is derived from an integral representation of the solution that we obtain by generalizing similar representations for the Stokes flow [12,13]. The representation allows us to derive the far flow consistently. It was assumed that the impact of a

particle on the flow can be represented by a point force only with the strength given by the Stokes force of unstratified flow [10]. In fact, the complete drag force with the stratification corrections must be used, and the far flow also includes the thermal component of the fundamental solution, which is the flow caused by the point source of heat. These corrections could be neglected for the lowest order [10]; however, they are necessary for higher-order studies. We derive the complete fundamental solution of the problem that includes the heat source.

A full understanding of the structure of the stratified flow around the sedimenting particle requires consideration of a flow component that was previously disregarded. This component is quite unique. It also exists when both the particle and the fluid at infinity are completely at rest. We call this flow "insulating" because its role is to screen the particle from the external gradients of the density that do not fit the heat boundary condition on the particle's surface. The insulating flow applies zero force on the particle and provides a steady-state solution for neutrally buoyant particles. This steady state appears to contradict the phenomenon of thermophoresis: a neutrally buoyant particle must move at a constant drift velocity that is proportional to the temperature gradient. Thermophoresis, however, is a kinetic phenomenon, and its description necessitates going beyond the standard fluid mechanical description by introducing a finite slip in the boundary conditions or otherwise; see [14,15] and the references therein. In this work, we confine the study to the effects captured by the continuum hydrodynamic description with no-slip boundary conditions. In the linear regime, thermophoretic correction of the settling velocity obtained in this way can be included by superposition. For sedimenting particles that are not neutrally buoyant, the flow is a superposition of the insulating flow and the flow caused by the finite settling velocity. Quantitatively, the insulating flow is usually small, and it seems to be relevant only for neutrally buoyant particles. Its most practical application can be to floating bodies, with appropriate changes necessitated by the nonspherical shape of the immersed part. Qualitatively, recognition of the presence of this component is necessary for completeness.

We confirmed our predictions at small Reynolds, Péclet, and up to order-1 Rayleigh numbers by numerical simulations. We also used the simulations to study the range of parameters where the equations are not linear and for which therefore no theory is available. We studied the range of Reynolds numbers up to 10 and Rayleigh numbers up to 1, the choice being dictated by the applications to the sinking of nonswimming plankton particles and organic particles of the marine snow [2,3]. Though the precise numbers depend on the application, we think mainly of particles with a size of the order of 1 mm or less. The Péclet number was fixed by using three representative values of the Prandtl number, 0.72, 7, and 700, describing the cases where the stratified agent is temperature. Despite the practical applicability of the considered range of dimensionless parameters, it has not been studied much, as stressed in [10]; see also [16]. We studied the drag force and the structure of the flow. Our numerical method is based on a monolithic velocity component decoupled projection method (FDMPM-1P) for mixed convection problems in a spherical coordinate system [17]. We compare the flow with the available previous numerical results.

Flows around a moving object in a stratified environment where the Reynolds number is nonsmall have been studied by many researchers. Torres *et al.* [18,19] experimentally and numerically observed the drag enhancement due to the stratification at Reynolds numbers larger than ten and found a vertical jet structure behind the sphere. The rear jet formation process was investigated intensely in [16,20–22]. It is stressed that the jet can attain velocities more than 5 times higher than the velocity of the sphere itself [16]. The smallest Reynolds number in the study was close to 100. Besides the case of a uniform density gradient considered in this paper, layered structures were studied, stressing the effect of a density change. A particle in a sharp density interface of a two-layer fluid was experimentally studied by Sridić-Mitrović *et al.* [23]. It was found that in a stably stratified fluid for the low-Reynolds-number case ($1.5 \leqslant \mathrm{Re} \leqslant 15$), the drag on a particle increased compared to that of the homogeneous fluid case due to the dragging of a lighter fluid to the particle. Camassa *et al.* [24,25] both experimentally and theoretically investigated undershoot of the terminal velocity of the bottom layer for the low-Reynolds-number case. For moderate Reynolds numbers,

Abaid *et al.* [26] observed an oscillation and levitation of a sphere after it crossed the density interface. The settling process of a sphere in a sharp density interface [27] and a linearly stratified fluid [28,29] is significantly affected by the presence of stratification. Similar configurations with different particles (elongated particle [30], a pair of particles [31], drop [32,33], and porous particle [34–36]) have been extensively studied. Recently, the inertial effect of stratification on a settling sphere was investigated using an asymptotic expansion by considering the Oseen-type correction [37], and the core mechanism of drag enhancement was numerically studied [38]. All these and other works do not seem to provide the main result of our work at small-Reynolds-number flow: accurate prediction of the enhancement of the drag coefficient as a function of Reynolds and Rayleigh numbers.

The paper is organized as follows: In Sec. II, the governing equations in the particular choice of moving frame and the numerical method adopted in our study are introduced. In Sec. III, the solution for small parameters such as the Reynolds number and Rayleigh number is described using an integral representation. The numerical results for nonsmall Reynolds numbers are provided with confirmation of the theoretical prediction at low Reynolds numbers in Sec. IV. Section V concludes the study.

II. FRAMEWORK

We consider motion at a constant velocity $-U_\infty \hat{z}$ of an isolated sphere with diameter d in an infinite fluid. The direction of the z axis is chosen as opposite to the direction of the gravitational acceleration vector, $\boldsymbol{g} = -g\hat{z}$. The fluid is assumed to be stratified so that in the absence of the sphere the temperature Θ^* would have a constant derivative in the z direction, $\gamma = \partial_z \Theta^* = Const$. Here γ is a positive constant corresponding to stratification with the colder and heavier fluid below. We assume that the interaction of the flow velocity $\boldsymbol{u}^*$ with the temperature can be described using the Boussinesq approximation:

$$\frac{\partial \boldsymbol{u}^*}{\partial t} + (\boldsymbol{u}^* \cdot \nabla)\boldsymbol{u}^* = -\frac{1}{\rho}\nabla p^* + \nu \nabla^2 \boldsymbol{u}^* + \beta g \Theta^* \hat{z},$$
$$\frac{\partial \Theta^*}{\partial t} + (\boldsymbol{u}^* \cdot \nabla)\Theta^* = \kappa \nabla^2 \Theta^*, \quad \nabla \cdot \boldsymbol{u}^* = 0, \tag{1}$$

where p^* is the pressure, and β, ν, κ, and ρ are the thermal expansion coefficient, kinematic viscosity, thermal diffusivity, and fluid density, respectively. A variable with the superscript * is a dimensional variable. This system of equations is completed with the boundary conditions on the surface S of the sphere and at infinity:

$$\boldsymbol{u}^*|_S = -U_\infty \hat{z}, \quad \partial_r \Theta^*|_S = 0, \quad \boldsymbol{u}^*_\infty = 0, \quad \Theta^*_\infty = \Theta^*_0 + \gamma z, \tag{2}$$

where the first equation expresses the no-slip boundary condition. The asymptotic values of the fields at infinity are designated by the subscript, and Θ^*_0 is a constant. We assume that the surface of a particle is thermally insulated so that the heat flux through S is zero and the Neumann boundary condition $\partial_r \Theta^*|_S = 0$ holds (this can also correspond to the impermeability condition if Θ^* describes the concentration). This boundary condition is usually used; see the discussion in [28]. The following calculations also usually apply to the Dirichlet boundary condition. For instance, the reciprocal theorem that follows has the same form for both types of boundary conditions.

A. Dimensionless equations in moving frame

For numerical simulations, it is useful to pass to the frame of the particle where the particle boundary is stationary. Thus, we pass to the frame that moves with the velocity of the particle, $-U_\infty \hat{z}$. In this frame, Eqs. (1) hold with the boundary conditions $\boldsymbol{u}^*(r = d/2) = 0$ and $\partial_r \Theta^*(r = d/2) = 0$ (we use the same notation for the fields in the moving frame, where no ambiguity can arise). The conditions at infinity are $\boldsymbol{u}^*_\infty = U_\infty \hat{z}$ and $\Theta^*_\infty = \Theta^*_0 + \gamma z - \gamma U_\infty t$. We introduce

$\Theta^{*\prime}(\mathbf{x}, t)$ describing deviations from the behavior at infinity:

$$\Theta^*(\mathbf{x}, t) = \Theta_0^* + \gamma z - \gamma U_\infty t + \Theta^{*\prime}(\mathbf{x}, t), \tag{3}$$

where $\Theta^{*\prime}$ vanishes at infinity. In terms of $\Theta^{*\prime}(\mathbf{x}, t)$, the equations in the moving frame are as follows:

$$\begin{aligned} &\frac{\partial \boldsymbol{u}^*}{\partial t} + (\boldsymbol{u}^* \cdot \nabla)\boldsymbol{u}^* = -\frac{1}{\rho}\nabla p' + \nu \nabla^2 \boldsymbol{u}^* + \beta g \Theta^{*\prime} \hat{z}, \\ &\frac{\partial \Theta^{*\prime}}{\partial t} + (\boldsymbol{u}^* \cdot \nabla)\Theta^{*\prime} + \gamma(u_z^* - U_\infty) = \kappa \nabla^2 \Theta^{*\prime}, \quad \nabla \cdot \boldsymbol{u}^* = 0, \end{aligned} \tag{4}$$

where p', the modified pressure, is given by $p^* - \rho\beta g \Theta_0^* z - \rho\beta\gamma g z^2/2 + \rho\gamma U_\infty t \beta g z$. The corresponding boundary conditions are time independent:

$$\boldsymbol{u}^*\left(|\boldsymbol{x}| = \frac{d}{2}\right) = 0, \quad \partial_r \Theta^{*\prime}\left(|\boldsymbol{x}| = \frac{d}{2}\right) = -\frac{2\gamma z}{d}, \quad \boldsymbol{u}_\infty^* = U_\infty \hat{z}, \quad \Theta^{*\prime}{}_\infty = 0, \tag{5}$$

and therefore the time-derivative terms in the equations can be omitted after the transients. We pass to dimensionless variables using

$$\boldsymbol{u}\left(\frac{\boldsymbol{x}}{d}, \frac{U_\infty t}{d}\right) = \frac{\boldsymbol{u}^*(\boldsymbol{x}, t)}{U_\infty}, \quad p\left(\frac{\boldsymbol{x}}{d}, \frac{U_\infty t}{d}\right) = \frac{p'(\boldsymbol{x}, t)}{\rho U_\infty^2}, \quad T\left(\frac{\boldsymbol{x}}{d}, \frac{U_\infty t}{d}\right) = \frac{\Theta^{*\prime}(\boldsymbol{x}, t)}{\gamma d}. \tag{6}$$

The dimensionless fields obey the following:

$$\frac{\partial \boldsymbol{u}}{\partial t} + (\boldsymbol{u} \cdot \nabla)\boldsymbol{u} = -\nabla p + \frac{1}{\mathrm{Re}}\nabla^2 \boldsymbol{u} + \frac{\mathrm{Ra}}{\mathrm{Re\,Pe}} T \hat{z}, \quad \frac{\partial T}{\partial t} + (\boldsymbol{u} \cdot \nabla)T + u_z - 1 = \frac{1}{\mathrm{Pe}}\nabla^2 T, \quad \nabla \cdot \boldsymbol{u} = 0. \tag{7}$$

The system is characterized by three dimensionless numbers: the Reynolds number Re, the Rayleigh number Ra, and the Péclet number Pe, which are defined by

$$\mathrm{Re} = \frac{U_\infty d}{\nu}, \quad \mathrm{Ra} = \frac{g\beta\gamma d^4}{\kappa\nu}, \quad \mathrm{Pe} = \frac{U_\infty d}{\kappa}, \tag{8}$$

respectively. Other dimensionless numbers can be obtained as functions of the above three numbers. The dimensionless Prandtl number $\mathrm{Pr} = \nu/\kappa$ obeys $\mathrm{Re\,Pr} = \mathrm{Pe}$. The Richardson number [10] is proportional to Ra/Pe.

The physical meaning of Re and Pe is well known: they measure the relative magnitude of the nonlinear and the diffusion of the momentum or scalar terms in the momentum and scalar equations, respectively. The Rayleigh number measures the ratio of the buoyancy and viscous friction forces in the momentum equation. We observe that the role of the buoyancy term grows with the scale, and the terms have the same order at the characteristic length:

$$L = \left(\frac{\kappa\nu}{N^2}\right)^{1/4}, \quad N^2 = g\beta\gamma, \tag{9}$$

where N is the Brunt-Väisälä frequency. The scale L, called the Rayleigh scale, is the crossover length beyond which the buoyancy dominates the flow, and $\mathrm{Ra} = d^4/L^4$ tells us whether this scale is larger than d. Hereafter, the nondimensionalized Rayleigh scale L/d will be denoted by $\mathrm{Ra}^{-1/4}$. At $\mathrm{Ra}^{1/4} \ll 1$, the flow at $1/2 \leqslant r \ll \mathrm{Ra}^{-1/4}$ is similar to the flow without buoyancy, except for the special case $U_\infty = 0$ considered in the next section (this scale separation used in [10] is a rather stringent assumption). At low Reynolds numbers, the flow decays fast beyond L as compared with the slow decay of the Stokes flow proportional to x^{-1}: see [5,7] and below.

The boundary conditions on the dimensionless fields are as follows:

$$\boldsymbol{u}\left(|\boldsymbol{x}| = \frac{1}{2}\right) = 0, \quad \partial_r T\left(|\boldsymbol{x}| = \frac{1}{2}\right) = -2z, \quad \boldsymbol{u}_\infty = \hat{z}, \quad T_\infty = 0. \tag{10}$$

The rescaling that we used above is not suited for the insulating flow considered separately in Sec. III A.

B. Numerical method

In the numerical part of the present study, an axisymmetric flow around a sedimenting sphere is simulated in the spherical coordinate system by using a monolithic velocity component decoupled projection method (FDMPM-1P) for mixed convection problems [17,39]. In this method, the Crank-Nicolson scheme is employed for discretizing the buoyancy, nonlinear convection, and linear diffusion terms in time by linearizing the nonlinear convection terms in both the momentum and energy equations. The Crank-Nicolson time advancement is employed for both convection and diffusion terms to avoid a severe Courant-Friedrichs-Lewy (CFL) time step restriction.

We performed numerical simulations of the system of Eqs. (7) with appropriate modification of the boundary conditions for the finite domain. In the spherical coordinate system, r, θ, and ϕ denote the radial, polar, and azimuthal directions, respectively. Because a falling sphere and the flow around the sphere in the low-Reynolds-number region has inherent axisymmetry, all azimuthal components ϕ were not considered in this study. The Dirichlet boundary condition ($\boldsymbol{u} = \hat{z}$ and $T = 0$) was used at the inflow boundary, and the convective boundary condition ($\partial\zeta/\partial t + c\partial\zeta/\partial z = 0$) was used at the outflow boundary, where $\zeta = u_x, u_z$, or T, and c is the space-averaged streamwise or axial velocity at the exit. Here, the inflow and outflow boundaries denote regions with $0 \leqslant \theta \leqslant \pi/2$ and $\pi/2 < \theta \leqslant \pi$, respectively. For the simulation of the insulating flow, we applied a different boundary condition, $\boldsymbol{u}_\infty = 0$.

Simulations are carried out in the parameter regime $0.005 \leqslant \mathrm{Re} \leqslant 10$, $10^{-5} \leqslant \mathrm{Ra} \leqslant 1$, and $\mathrm{Pr} = 0.72, 7$, and 700. The Cartesian coordinate system (x, y, z) is also used to represent the drag force and to implement the boundary condition at the outlet. The computational domain is $r_i(=1/2) \leqslant r \leqslant r_o(=30$ for $\mathrm{Re} > 1$ and 150 for $\mathrm{Re} \leqslant 1)$, $0 \leqslant \theta \leqslant \pi$. For accurate calculation of drag modification at low Reynolds numbers, a relatively large domain is selected. In the radial direction, the nonuniform grid points $r_m(m = 1, 2, ..., M)$ are given by

$$r_m = r_i + (r_o - r_i)\frac{s^{m-1} - 1}{s^{M-1} - 1}, \tag{11}$$

where s is the stretching ratio, and M is the number of radial grid points. The grids are constructed uniformly in the θ direction. In this study, the grid points are generated with $s = 1.072\,411\,5$, $M = 128$ (for $r_o = 30$) and $s = 1.094$, $M = 128$ (for $r_o = 150$), and $N = 256$, where N is the number of grid points in the θ direction. These domain sizes and grids were chosen so that the computed drag is insensitive to them. For example, when M is increased from 128 to 384, the drag changes by less than 0.02%, while when N is increased from 256 to 384, the drag changes by less than 0.02% for $\mathrm{Re} = 0.01$, $\mathrm{Ra} = 1$, and $\mathrm{Pr} = 0.72$, for which drag is most significantly modified by stratification among all cases.

III. RECIPROCAL THEOREM AND INTEGRAL REPRESENTATION FOR SLOW MOTION

In this section, we consider the flow in the limit of the small particle velocity U_∞, where Re and Pe defined in Eq. (8) become much lower than 1. Remarkably, the flow remains nonzero even at $U_\infty = 0$. This peculiar limiting flow does not apply a force on the particle, which is necessary for self-consistency. A discussion of this flow appears to be missing in the literature, despite the fact that it is also present at a nonzero U_∞ as a finite, though usually small, component of the total flow. An understanding of this component is necessary for a consistent view of the solution of the fluid mechanical equations. Thus, we start examining this flow in the following section. Then we consider the complete flow for nonzero U_∞ for the reciprocal theorem and the fundamental solution, including the drag modification in the subsequent subsections.

A. Insulating flow round a neutrally buoyant particle

The case of neutrally buoyant particles where the particle density ρ_p equals the fluid density ρ_f is a unique situation where the fluid at infinity and the particle are both at rest and yet there is a flow. This flow is driven by the buoyancy force due to a nontrivial distribution of temperature around the particle. That distribution cannot be reabsorbed in the pressure, in contrast with the linear distribution of density, which holds without the particle. We call the arising flow "insulating" because it originates in the nontrivial density distribution due to the insulating boundary condition. It helps to screen the particle from the outside density gradients so that the gradients on the particle surface have no radial component.

An understanding of the insulating flow is necessary for a complete understanding of the flow around a sedimenting (not neutrally buoyant) particle, which is considered in the next section. This is because this flow is a finite component of the total flow caused by the sedimenting particle. This component is typically negligible, even for the particles that are almost neutrally buoyant. For instance, this is the case of Volvox [40], which is reasonably well represented by the spherical shape studied here, and has a $\rho_p/\rho_f - 1$ of approximately 10^{-3}; see [40] for the role of sedimentation in Volvox's motion. The situation can be different in the case of turbulence, where much larger density gradients can occur. These gradients could make the insulating flow a non-negligible component of the perturbation of the turbulent flow caused by the particle. The study of turbulence is left for future work.

The insulating flow appears to be of practical interest only in the case of completely neutrally buoyant particles at rest. One universal application is the case of floating bodies. Despite the fact that these bodies are located at the surface and that the shape immersed in water is not a complete sphere, as considered in this section, our solution provides a good reference point for the study of this flow. The angular structure of our solution for a complete sphere probably applies in the case where the immersed portion is a part of the sphere. This is because of the axial symmetry that holds in both cases. For general immersed shapes, our solution can be used for order-of-magnitude estimates. The insulating flow could also be relevant in the case of fish, which regulate their buoyancy by using a swim bladder in order to achieve neutrality at different depths.

We consider a nontrivial equilibrium solution of the nonlinear fluid mechanical equations where the particle does not move, $U_\infty = 0$, despite the existence of local gradients. The force that the fluid exerts on the particle is zero, which is necessary for the solution's self-consistency. The dimensionless variables introduced in Sec. II are not suitable for this study; therefore, we consider the original Eqs. (1). It is simpler to demonstrate the existence of the insulating flow solution by using $\tilde{\Theta} = \Theta^* - \Theta_0^*$ and $\tilde{p} = p^* - \rho\beta g\Theta_0^* z$, that obey in the steady state,

$$(\boldsymbol{u}^*\cdot\nabla)\boldsymbol{u}^* = -\frac{1}{\rho}\nabla\tilde{p} + \nu\nabla^2\boldsymbol{u}^* + \beta g\tilde{\Theta}\hat{z}, \quad (\boldsymbol{u}^*\cdot\nabla)\tilde{\Theta} = \kappa\nabla^2\tilde{\Theta}, \quad \nabla\cdot\boldsymbol{u}^* = 0. \tag{12}$$

The symmetry of the corresponding boundary conditions,

$$\boldsymbol{u}^*|_S = 0, \quad \partial_r\tilde{\Theta}|_S = 0, \quad \boldsymbol{u}^*_\infty = 0, \quad \tilde{\Theta}_\infty = \gamma z, \tag{13}$$

implies the symmetry of the solution: $\tilde{\Theta}$ and $\boldsymbol{u}^*$ are odd functions of $\boldsymbol{r}$ and $\tilde{p}$ is even. We find that the $\tilde{\sigma}_{ik}$ component of the full stress tensor σ^*_{ik},

$$\sigma^*_{ik} = \rho\beta g\Theta_0^* z\delta_{ik} + \tilde{\sigma}_{ik}, \quad \tilde{\sigma}_{ik} = -\tilde{p}\delta_{ik} + \eta(\nabla_i u^*_k + \nabla_k u^*_i), \tag{14}$$

is an odd function of $\boldsymbol{r}$. Thus, the force $\int_{r=a}\sigma^*_{ik}dS_k$ that the fluid applies on the particle equals the buoyancy force determined by the uniform component Θ_0^* of Θ^*. We conclude that neutrally buoyant particles will not move in the presence of stratification or stable heat conduction. If the particle was moving initially, then this solution would apply after the transients.

It is useful to consider dimensionless fields and variables:

$$\boldsymbol{u}^*(\boldsymbol{x},t) = \frac{\kappa}{d}\boldsymbol{u}_i\left(\frac{\boldsymbol{x}}{d},\frac{\kappa t}{d^2}\right), \quad \frac{\tilde{p}(\boldsymbol{x},t)}{\rho} - \frac{\beta\gamma g z^2}{2} = \frac{\kappa^2}{d^2}p_i\left(\frac{\boldsymbol{x}}{d},\frac{\kappa t}{d^2}\right), \quad \tilde{\Theta}(\boldsymbol{x},t) - \gamma z = \gamma d\, T_i\left(\frac{\boldsymbol{x}}{d},\frac{\kappa t}{d^2}\right), \tag{15}$$

where the subscript i stands for "insulating." The dimensionless fields obey

$$\frac{\partial \boldsymbol{u}_i}{\partial t} + (\boldsymbol{u}_i \cdot \nabla)\boldsymbol{u}_i = -\nabla p_i + \mathrm{Pr}\nabla^2 \boldsymbol{u}_i + \mathrm{Ra}\,\mathrm{Pr}\, T_i \hat{z}, \quad \frac{\partial T_i}{\partial t} + (\boldsymbol{u}_i \cdot \nabla)T_i + (u_i)_z = \nabla^2 T_i,$$
$$\nabla \cdot \boldsymbol{u}_i = 0, \tag{16}$$

where we restored the time-derivative terms so that transients can be considered. In contrast with the solution considered in the previous section, which depends on three dimensionless parameters, the insulating flow solution depends only on two such parameters: Ra and Pr. The boundary conditions are

$$\boldsymbol{u}_i\left(r = \frac{1}{2}\right) = 0, \quad \partial_r T_i\left(r = \frac{1}{2}\right) = -2z, \quad \boldsymbol{u}_i(\infty) = 0, \quad T_i(\infty) = 0. \tag{17}$$

We observe that at $\mathrm{Ra} \ll 1$ the equations become linear, because the velocity $\boldsymbol{u}_i$ becomes proportional to the small parameter Ra in front of the source term in the momentum equation. In this case, the terms of the scalar equation involving the velocity are small so that in the steady state T_i obeys the Laplace equation. The solution is the harmonic function that fits the boundary condition in Eq. (17),

$$T_i = \frac{z}{16r^3}, \quad \nabla^2 T_i = 0. \tag{18}$$

The nonlinear term in the momentum equation is negligible and the velocity obeys

$$-\nabla p_i' + \nabla^2 \boldsymbol{u}_i = -\boldsymbol{\phi}, \quad \boldsymbol{\phi} = \mathrm{Ra} T_i \hat{z} = \frac{\mathrm{Ra} z \hat{z}}{16r^3}, \quad \boldsymbol{u}_i\left(r = \frac{1}{2}\right) = \boldsymbol{u}_i(\infty) = 0, \tag{19}$$

where $p_i' = p_i/\mathrm{Pr}$ and $\nabla \cdot \boldsymbol{u}_i = 0$. Thus, indeed, the velocity is proportional to Ra, which determines the amplitude of the source. However, this approximation cannot be transformed into a globally valid solution because the source decays at infinity only as r^{-2}. The reason is that the Laplacian of a function decaying at infinity decays faster than r^{-2}; therefore, the equation on $\boldsymbol{u}_i$ with the above source cannot have a solution decaying at infinity (the pressure term cannot correct this because the source is not potential). The other, more explicit way to see the difficulty is to write the formal solution of Eq. (19) with the help of the fundamental Stokeslet solution of Stokes equations outside a rigid sphere; see, e.g., [41] and the references therein:

$$u_l(\boldsymbol{x}) = \frac{\mathrm{Ra}}{128\pi} \int_{|\boldsymbol{x}'|>1/2} \frac{G_{lz}(\boldsymbol{x}, \boldsymbol{x}')z'}{r'^3} d\boldsymbol{x}', \tag{20}$$

where $G_{ik}(\boldsymbol{x}, \boldsymbol{x}')$ represents the solution of the linear Stokes equations with point force,

$$-\nabla p_s + \nabla^2 \boldsymbol{u}_s = -\boldsymbol{F}\delta(\boldsymbol{x} - \boldsymbol{x}'), \quad \nabla \cdot \boldsymbol{u}_s = 0, \quad \boldsymbol{u}_s\left(r = \frac{1}{2}\right) = \boldsymbol{u}_s(\infty) = 0,$$
$$\boldsymbol{u}_s(\boldsymbol{x}) = \frac{G_{ik}(\boldsymbol{x}, \boldsymbol{x}')F_k}{8\pi}. \tag{21}$$

The fundamental solution $G_{lz}(\boldsymbol{x}, \boldsymbol{x}')$ exhibits the same $|\boldsymbol{x} - \boldsymbol{x}'|^{-1}$ behavior at large distances from the source as the Stokeslet solution in the infinite space as given by the Oseen tensor [12,41]. Thus, the quadratic decay of $T_i(\boldsymbol{x}')$ in the integrand in Eq. (20) is too slow, and the integral diverges logarithmically (faster than quadratic decay would already give a global solution). This demonstrates the insolvability of the problem set by Eq. (19). The origin of the problem is that the velocity term in the scalar equation stops to be a small perturbation at large distances. The power counting in Eq. (19) gives that the exponent providing the scaling of $(u_i)_z$ in r is zero (the solution is of logarithmic type). Correspondingly, the account of the $(u_i)_z$ term in the heat equation induces the correction in the temperature that behaves as r^2 Ra. However, the ratio of this term to the zero-order solution given by Eq. (18) grows with r as r^4 Ra. Therefore this term becomes non-negligible at

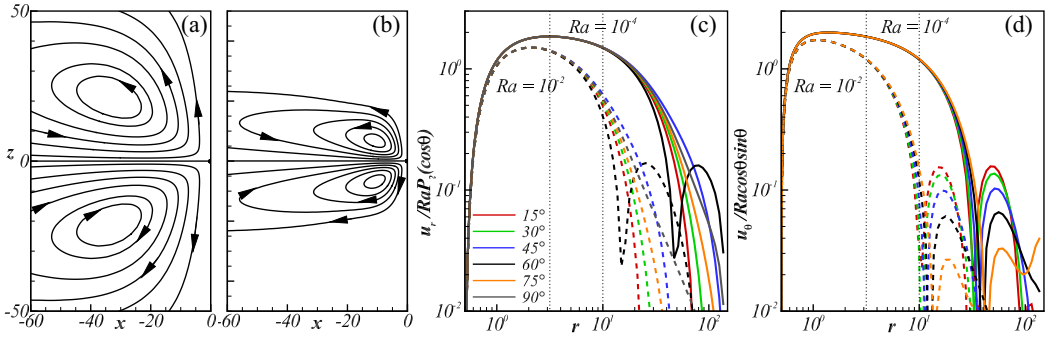

FIG. 1. Streamlines of insulating flow for (a) $\mathrm{Ra} = 10^{-4}$ and (b) $\mathrm{Ra} = 10^{-2}$, and the compensated velocity components, (c) $u_{ir}/[\mathrm{Ra}P_2(\cos\theta)]$ and (d) $u_{i\theta}/(\mathrm{Ra}\sin\theta\cos\theta)$. In (a) and (b), the sphere is located at the origin. The compensated velocity components are plotted for six different angles, 15, 30, 45, 60, 75, and 90°, and collapse on the same curve for moderate r/d. The vertical line indicates $L/d = \sqrt{10}$ and 10 for $\mathrm{Ra} = 10^{-2}$ and $\mathrm{Ra} = 10^{-4}$, respectively.

r determined by the condition $r^4\,\mathrm{Ra} \sim 1$, which in dimensional variables is the Rayleigh scale L introduced in Eq. (9) of the previous section. The globally valid solution can be determined only by solving the complete system

$$0 = -\nabla p_i + \mathrm{Pr}\,\nabla^2 \boldsymbol{u}_i + \mathrm{Ra}\,\mathrm{Pr}\,T_i\hat{z}, \quad (u_i)_z = \nabla^2 T_i, \quad \nabla\cdot\boldsymbol{u}_i = 0, \tag{22}$$

where we retained the $(u_i)_z$ term in Eqs. (16). The flow decays fast at $r > L$, as can be seen by taking the Laplacian of the momentum equation and using the scalar equation [7]. This results in the generalized bi-Helmholtz equation

$$\nabla\nabla^2 p' = \mathrm{Ra}\,u_z\hat{z} + \nabla^4\boldsymbol{u}, \tag{23}$$

where $p' = p_i/\mathrm{Pr}$. The right-hand side indicates exponential-type solutions that behave as $\exp(-c\,\mathrm{Ra}^{1/4}|\boldsymbol{x}|)$ with a positive constant c of order 1. Indeed, fast decay of the solution beyond the Rayleigh scale L, given in dimensionless variables by $\mathrm{Ra}^{-1/4}$, is proved below using the fundamental solution of Eq. (22). That solution can be derived, and its fast decay at $r > \mathrm{Ra}^{-1/4}$ was demonstrated numerically in [5] and theoretically in [7]. Because the flow at $r \lesssim \mathrm{Ra}^{-1/4}$ is of order Ra and it decays fast at $r > \mathrm{Ra}^{-1/4}$, at $\mathrm{Ra} \ll 1$, the maximum of the flow magnitude is of order Ra. This proves the self-consistency of neglecting in Eq. (22) the nonlinear terms of Eq. (16).

The angular structure of the flow can be obtained at $\mathrm{Ra}^{1/4} \ll 1$, where there is a range of scales r that are much smaller than the Rayleigh scale, $r \ll \mathrm{Ra}^{-1/4}$. We demonstrate in Sec. I of the Supplemental Material [42] that various theoretical arguments point to the angular structure of the flow given by

$$u_{ir} = \mathrm{Ra}\,f(r)P_2(\cos\theta), \quad u^h_{i\theta} = \mathrm{Ra}\,h(r)\sin\theta\cos\theta, \tag{24}$$

where $P_2(x)$ is a Legendre polynomial of the second order, and f and h are functions of r that obey $f(r = 1/2) = h(r = 1/2) = 0$ and whose form is determined by the matched asymptotic study of $r \sim \mathrm{Ra}^{-1/4}$. To test these angular distributions of the velocity, we carried out a full numerical simulation solving the complete governing equations with the nonlinear terms [Eqs. (16)] and the boundary conditions [Eqs. (17)] in the domain $1/2 \leqslant r \leqslant 150$, at $\mathrm{Re} = 0.01$ and $\mathrm{Ra} = 10^{-4}, 10^{-2}$. Figure 1 demonstrates the streamline distribution of the resulting flow and the radial distribution of the compensated velocity components. The sphere located at the origin through buoyancy creates a circulatory motion that extends far from the sphere. The angular structure of Eq. (24) is indeed confirmed in the region $r < \mathrm{Ra}^{-1/4}$ for each Rayleigh number by the numerical simulations.

The characteristic value of the velocity of the insulating flow is seen to be $\kappa\ \mathrm{Ra}/d$. We compare this value with the characteristic value of the flow of a sedimenting (not neutrally buoyant) particle. We demonstrate below that the drag force is of the order of the Stokes force at $\mathrm{Ra} \lesssim 1$. Thus, the typical velocity of the flow caused by the sedimentation has the usual Stokes' value $(\rho_p - \rho_f)d^2/(18\nu\rho_f)$. It is readily seen that except for the particles that are very close to being neutrally buoyant, the latter value is much larger than the insulating flow. Below we consider the case of particles that are not neutrally buoyant and assume $U_\infty > 0$ with no loss, which is the case with heavy particles. The solution for $U_\infty < 0$ that is applicable to light particles or swimmers can be found by transformation of the parameters of the solution for $U_\infty > 0$; see Sec. II of the Supplemental Material [42]. We will see that though the insulating flow contribution in the total flow is small, it is necessary for a conceptual understanding of the solution.

B. Sedimentation

From this point on we consider the flow induced by a sphere that sediments in stratified fluid at a finite velocity. We assumed in the previous section that at the considered Ra and Pr the insulating flow can be described by Eqs. (22), which are linear. Here, we assume that the sedimentation velocity provides for Re and Pe much smaller than 1. Under these assumptions, the flow around the sedimenting particle is well described by linear fluid mechanics. We use the fluid frame of reference for the study considering Eqs. (1). We neglect the left-hand side of the first of Eqs. (1) using $\mathrm{Re} \ll 1$. In contrast, we cannot neglect the left-hand side of the second of Eqs. (1) using $\mathrm{Pe} \ll 1$, because Θ^* contains the linear term γz, which does not contribute to the Laplacian of Θ^* but does produce a non-negligible contribution in the convective term $(\boldsymbol{u}^* \cdot \nabla)\Theta^*$. To utilize the smallness of Pe, we introduce $\theta^* = \Theta^* - \Theta_0^* - \gamma z$, where $\partial_r\theta^*$ on the surface of the sphere is $-2\gamma z/d$. The system of Eqs. (1) becomes

$$\nabla P = \nu\nabla^2\boldsymbol{u}^* + \beta g\theta^*\hat{z}, \quad \partial_t\theta^* + (\boldsymbol{u}^* \cdot \nabla)\theta^* + \gamma u_z^* = \kappa\nabla^2\theta^*, \quad \nabla \cdot \boldsymbol{u}^* = 0, \tag{25}$$

where $P^* = p^*/\rho - \beta g\Theta_0^* z - \beta\gamma g z^2/2$. Here we can already use $\mathrm{Pe} \ll 1$ and neglect $\partial_t\theta^* + (\boldsymbol{u}^* \cdot \nabla)\theta^*$ in the second equation in comparison with the Laplacian term, $\gamma u_z^* \approx \kappa\nabla^2\theta^*$. We introduce dimensionless variables that are somewhat different from Eq. (6):

$$\boldsymbol{u}^* = U_\infty \boldsymbol{u}\left(\frac{\boldsymbol{x}}{d}\right), \quad P = \frac{\nu U_\infty}{d} p\left(\frac{\boldsymbol{x}}{d}\right), \quad \theta^* = \frac{\gamma U_\infty d^2}{\kappa}\theta\left(\frac{\boldsymbol{x}}{d}\right), \tag{26}$$

cf. [10]. The system of Eqs. (25) becomes

$$\nabla p = \nabla^2\boldsymbol{u} + \mathrm{Ra}\theta\hat{z}, \quad u_z = \nabla^2\theta, \quad \nabla \cdot \boldsymbol{u} = 0, \quad \boldsymbol{u}\left(|\boldsymbol{x}| = \frac{1}{2}\right) = \boldsymbol{v}, \quad \partial_r\theta\left(|\boldsymbol{x}| = \frac{1}{2}\right) = -\frac{2z}{\mathrm{Pe}}, \tag{27}$$

with both fields vanishing at infinity. The boundary condition corresponding to the sedimentation is $\boldsymbol{v} = -\hat{z}$. Here, we included the horizontal motions of the particle by allowing an arbitrary $\boldsymbol{v}$. The Rayleigh number is a coupling constant so that the velocity decouples from the scalar at $\mathrm{Ra} = 0$. The construction of the perturbation theory in Ra that starts with the Stokes flow as the zero-order solution is not trivial, though. This theory is not analytic, because different signs of γ correspond to different physics, and $\mathrm{Ra} = 0$ is a singular point when the solution's dependence on Ra is considered. Indeed, it is seen below that the expansion parameter is $\mathrm{Ra}^{1/4}$, which is ill-defined at $\mathrm{Ra} < 0$. Moreover, as described in the previous section, the flow beyond the Rayleigh scale $\mathrm{Ra}^{-1/4}$ is fast decaying, so that the correction to the Stokes flow, decaying only as a power law, is not small.

The solution of Eqs. (27) is a superposition of the solutions caused by the boundary conditions on $\boldsymbol{u}$ and θ separately:

$$\boldsymbol{u} = \boldsymbol{u}_1 + \boldsymbol{u}_2, \quad p = p_1 + p_2, \quad \theta = \theta_1 + \theta_2, \tag{28}$$

where both $\boldsymbol{u}_i$ and θ_i vanish at infinity and obey

$$\begin{aligned}
&\nabla p_1 = \nabla^2 \boldsymbol{u}_1 + \mathrm{Ra}\theta_1 \hat{z}, \quad u_{1z} = \nabla^2 \theta_1, \quad \nabla \cdot \boldsymbol{u}_1 = 0, \\
&\boldsymbol{u}_1\left(|\boldsymbol{x}| = \frac{1}{2}\right) = \boldsymbol{v}, \quad \partial_r \theta_1\left(|\boldsymbol{x}| = \frac{1}{2}\right) = 0, \\
&\nabla p_2 = \nabla^2 \boldsymbol{u}_2 + \mathrm{Ra}\theta_2 \hat{z}, \quad u_{2z} = \nabla^2 \theta_2, \quad \nabla \cdot \boldsymbol{u}_2 = 0, \\
&\boldsymbol{u}_2\left(|\boldsymbol{x}| = \frac{1}{2}\right) = 0, \quad \partial_r \theta_2\left(|\boldsymbol{x}| = \frac{1}{2}\right) = -\frac{2z}{\mathrm{Pe}}.
\end{aligned} \tag{29}$$

We see that $\boldsymbol{u}_2$ is the insulating flow considered previously, which is rescaled because different dimensionless parameters are used. Because this flow applies no force on the particle, for the purpose of finding the force on the particle, we may concentrate on the flow $\boldsymbol{u}_1$ in the first line of Eqs. (29). This form of the problem of finding the force seems to be the simplest.

The flow determined by Eqs. (29) is quite complex and probably cannot be solved completely. Nevertheless, much progress is possible. We introduce an integral representation of the solution that we derive from a modified Lorentz identity [9] and a reciprocal theorem. The identity is found by observing that if $\tilde{\boldsymbol{u}}$ and $\tilde{\theta}$ provide another solution of Eqs. (27) with the stress tensor $\tilde{\sigma}_{ik}$, then

$$\nabla_k(u_i \tilde{\sigma}_{ik}) - \mathrm{Ra}\, \nabla \cdot (\theta \nabla \tilde{\theta}) = \nabla_k(\tilde{u}_i \sigma_{ik}) - \mathrm{Ra}\, \nabla \cdot (\tilde{\theta} \nabla \theta), \tag{30}$$

which can be confirmed by differentiation, using Eqs. (27) and standard transformations [12]. By integrating this equation over the volume of the flow outside the sphere, we find the reciprocal theorem

$$\int u_i \tilde{\sigma}_{ik} dS_k - \mathrm{Ra} \int \theta \partial_r \tilde{\theta} dS = \int \tilde{u}_i \sigma_{ik} dS_k - \mathrm{Ra} \int \tilde{\theta} \partial_r \theta dS, \tag{31}$$

where dS_k points in the radial direction: cf. [9,12]. A version of this identity with the reciprocal flow given by the fundamental solution leads to the integral representation.

We introduce the fundamental Stokeslet solution of our equations,

$$\nabla p' = \mathrm{Ra}\, \theta' \hat{z} + \nabla^2 \boldsymbol{u}' + \boldsymbol{g}\delta(\boldsymbol{x} - \boldsymbol{x}_0), \quad u'_z = \nabla^2 \theta' + s\delta(\boldsymbol{x} - \boldsymbol{x}_0), \tag{32}$$

where $\boldsymbol{g}$ and s are constant vector and scalar quantities, respectively, cf. Eq. (21). We will demonstrate that, as in other linear fluid mechanical problems [12], this solution provides the far field form of the solution of Eqs. (27). It is the result of rigorous calculations below that the effect of the insulating boundary condition on the particle surface on the fluid mechanical fields at large distances is equivalent to that of a heat source. This necessitates the introduction of the s term in Eqs. (32). In fact, an example was already provided in the previous section: it is seen readily that the solution given by Eq. (18), when extended to the interior of the particle, obeys the Laplace equation with the source proportional to $\nabla_z \delta(\boldsymbol{x})$.

Fundamental solution with s in Eqs. (32) set to zero was introduced in [5], where it was solved in Fourier space. The inverse Fourier transform performed numerically demonstrated that the solution decays fast beyond the Rayleigh scale $\mathrm{Ra}^{-1/4}$. A quantitative description was given in [7], where it was demonstrated that the decay at large distances r from the origin is not slower than r^{-9}.

The fundamental solution is a function of $\boldsymbol{x} - \boldsymbol{x}_0$ so we set $\boldsymbol{x}_0 = 0$ with no loss of generality. The solution can be represented as

$$u'_i(\boldsymbol{x}) = \frac{G_{ik}(\boldsymbol{x}) g_k}{8\pi} + \frac{\tilde{G}_i(\boldsymbol{x}) s}{8\pi}, \quad \theta'(\boldsymbol{x}) = \frac{\Theta_k(\boldsymbol{x}) g_k}{8\pi} + \frac{\tilde{\Theta}(\boldsymbol{x}) s}{8\pi}, \quad p'(\boldsymbol{x}) = \frac{P_k(\boldsymbol{x}) g_k}{8\pi} + \frac{\tilde{P}(\boldsymbol{x}) s}{8\pi}, \tag{33}$$

where G, $\tilde{G}$, Θ, $\tilde{\Theta}$, $\tilde{P}_i$, and $\tilde{P}$ are independent of $\boldsymbol{g}$ and s. We used the linearity of the equations and provided definitions similar to those for unstratified flows [9,12,13]. The introduced functions obey reciprocal relations that are derived in the same way as for unstratified flows [13]:

$$G_{ik}(\boldsymbol{x}) = G_{ki}(-\boldsymbol{x}), \quad \tilde{\boldsymbol{G}}(\boldsymbol{x}) = -\,\mathrm{Ra}\, \boldsymbol{\Theta}(-\boldsymbol{x}) : \quad \tilde{\Theta}(\boldsymbol{x}) = \tilde{\Theta}(-\boldsymbol{x}), \tag{34}$$

see Sec. III of the Supplemental Material [42]. The first of the above relations also holds for the Green function of the unstratified Stokes equation [13]. The reciprocal relation in the stratified case is considerably more informative; it tells that the ith component of flow caused at $\boldsymbol{x}$ by a unit point source of heat at the origin equals the product of minus Ra and the temperature at $-\boldsymbol{x}$ caused by a unit force in the ith direction at the origin. These relations are a form of the Onsager reciprocal relations for small deviations from the equilibrium stratified state.

The Lorentz-type identity for a solution of Eqs. (27) and the fundamental solution takes the form

$$\mathrm{Ra}\, s\theta\delta(\boldsymbol{x}'-\boldsymbol{x})-\boldsymbol{u}\cdot\boldsymbol{g}\delta(\boldsymbol{x}'-\boldsymbol{x})=\nabla'_k(u_i\sigma'_{ik})-\nabla'_k(u'_i\sigma_{ik})-\ \mathrm{Ra}\,\nabla'\cdot(\theta\nabla'\theta')+\mathrm{Ra}\ \ \nabla'\cdot(\theta'\nabla'\theta), \tag{35}$$

where we use $\boldsymbol{x}$ as the position of the source of the fundamental solution and $\boldsymbol{x}'$ as the spatial variable. The derivatives with respect to $\boldsymbol{x}'$ are designated by primes. We consider the source position $\boldsymbol{x}$ outside the sphere and perform spatial integration over $\boldsymbol{x}'$ outside the sphere. Upon the use of the reciprocal relations, this leads to the integral representations

$$\begin{aligned}
u_{1i}(\boldsymbol{x})&=\frac{v_z}{8\pi}\int_{r<1/2}\tilde{G}_i(\boldsymbol{x}-\boldsymbol{x}')d\boldsymbol{x}'-\nabla\cdot\int_{r=1/2}\hat{r}'\theta_1(\boldsymbol{x}')\tilde{G}_i(\boldsymbol{x}-\boldsymbol{x}')\frac{dS'}{8\pi}\\
&\quad-\int_{r=1/2}G_{ik}(\boldsymbol{x}-\boldsymbol{x}')\sigma_{1kr}(\boldsymbol{x}')\frac{dS'}{8\pi},\\
\theta_1(\boldsymbol{x})&=-\frac{1}{8\pi}\int_{r=1/2}\Theta_i(\boldsymbol{x}-\boldsymbol{x}')\sigma_{1ir}(\boldsymbol{x}')dS'+\frac{v_z}{8\pi}\int_{r<1/2}\tilde{\Theta}(\boldsymbol{x}-\boldsymbol{x}')d\boldsymbol{x}'-\frac{1}{8\pi}\nabla\\
&\quad\cdot\int_{r=1/2}\hat{r}'\theta_1(\boldsymbol{x}')\tilde{\Theta}(\boldsymbol{x}-\boldsymbol{x}')dS',
\end{aligned} \tag{36}$$

and

$$\begin{aligned}
u_{2i}(\boldsymbol{x})&=\int_{r'=1/2}\tilde{G}_i(\boldsymbol{x}-\boldsymbol{x}')\frac{\hat{z}'\cdot d\boldsymbol{S}}{8\pi\,\mathrm{Pe}}-\nabla\cdot\int_{r=1/2}\hat{r}'\theta_2(\boldsymbol{x}')\tilde{G}_i(\boldsymbol{x}-\boldsymbol{x}')\frac{dS'}{8\pi}\\
&\quad-\int_{r=1/2}G_{ik}(\boldsymbol{x}-\boldsymbol{x}')\sigma_{2kr}(\boldsymbol{x}')\frac{dS'}{8\pi},\\
\theta_2(\boldsymbol{x})&=\int_{r'=1/2}\tilde{\Theta}(\boldsymbol{x}-\boldsymbol{x}')\frac{\hat{z}'\cdot d\boldsymbol{S}}{8\pi\,\mathrm{Pe}}-\int_{r=1/2}\Theta_i(\boldsymbol{x}-\boldsymbol{x}')\sigma_{2ir}(\boldsymbol{x}')\frac{dS'}{8\pi}-\nabla\\
&\quad\cdot\int_{r=1/2}\hat{r}'\theta_2(\boldsymbol{x}')\tilde{\Theta}(\boldsymbol{x}-\boldsymbol{x}')\frac{dS'}{8\pi};
\end{aligned} \tag{37}$$

see the derivation in Sec. IV of the Supplemental Material [42]. (We keep the arbitrary value of v_z in the formulas for stressing the dependence on $\boldsymbol{v}$ in the boundary condition on velocity in Eq. (27). This can be set to minus 1; see the remark after Eq. (27). We keep the general v_z for making the dependence on it, which would hold in dimensional variables, transparent.) The boundaries represent distributed sources of the momentum and scalar similarly to unstratified flow [12]. In contrast to that flow, the interior of the sphere also provides scalar sources, because the source applies a finite force on a volume that does not enclose it:

$$\int_{r=1/2}\sigma'_{ir}(\boldsymbol{x}'-\boldsymbol{x})dS=-\mathrm{Ra}\,\delta_{iz}\int_{r<1/2}\theta'(\boldsymbol{x}'-\boldsymbol{x})d\boldsymbol{x}', \tag{38}$$

as can be seen from $\nabla_k\sigma_{ik}=-\ \mathrm{Ra}\,\theta'\hat{z}$. The velocity, besides the surface integral of the stress tensor similar to unstratified flow [12], includes contributions from the stratified agent. These contributions are both a surface and a volume integral.

C. Fundamental solution

In this section, we derive the Fourier transform of the fundamental solution and its asymptotic form at small distances. The Fourier transform of Eq. (32) gives ($\boldsymbol{x}_0 = 0$),

$$i\boldsymbol{k}p' = \mathrm{Ra}\,\theta'\hat{z} - k^2\boldsymbol{u}' + \boldsymbol{g}, \quad u_z' = -k^2\theta' + s. \tag{39}$$

We multiply the first equation by $\boldsymbol{k}$ and use the incompressibility condition $\boldsymbol{k}\cdot\boldsymbol{u}' = 0$ to eliminate the pressure:

$$p' = -\frac{i\,\mathrm{Ra}\,\theta' k_z}{k^2} - \frac{i\boldsymbol{k}\cdot\boldsymbol{g}}{k^2}. \tag{40}$$

Introducing $\hat{k} \equiv \boldsymbol{k}/k$ and the projection matrix $\Pi(\boldsymbol{k})$ leads to

$$k^2\boldsymbol{u}' = \mathrm{Ra}\,\theta'\Pi(\boldsymbol{k})\hat{z} + \Pi(\boldsymbol{k})\boldsymbol{g}, \quad \Pi_{ij}(\boldsymbol{k}) = \delta_{ij} - \hat{k}_i\hat{k}_j. \tag{41}$$

Plugging u_z' from the above formula into the equation on θ' and using $k_\perp^2 = k^2 - k_z^2$, we find

$$\begin{aligned} u_i' &= \frac{\Pi_{ik}(\boldsymbol{k})g_k}{k^2} - \frac{\mathrm{Ra}\,\Pi_{iz}(\boldsymbol{k})\Pi_{zk}(\boldsymbol{k})g_k}{k^6 + \mathrm{Ra}\,k_\perp^2} + \frac{k^2 s\,\mathrm{Ra}\,\Pi_{iz}(\boldsymbol{k})}{k^6 + \mathrm{Ra}\,k_\perp^2}, \\ \theta' &= -\frac{k^2\Pi_{zl}(\boldsymbol{k})g_l}{k^6 + \mathrm{Ra}\,k_\perp^2} + \frac{k^4 s}{k^6 + \mathrm{Ra}\,k_\perp^2}. \end{aligned} \tag{42}$$

This solution for $s = 0$ was derived in [4,5]; see also [7]. By comparing Eqs. (42) with Eqs. (33), we have for the components of the Green function of the velocity,

$$\begin{aligned} \frac{G_{ik}(\boldsymbol{k})}{8\pi} &= \frac{G^0_{ik}(\boldsymbol{k})}{8\pi} - \frac{\mathrm{Ra}\,\Pi_{iz}(\boldsymbol{k})\Pi_{zk}(\boldsymbol{k})}{k^6 + \mathrm{Ra}\,k_\perp^2}, \quad \frac{\tilde{G}_i(\boldsymbol{x})}{8\pi} = \frac{k^2\,\mathrm{Ra}\,\Pi_{iz}(\boldsymbol{k})}{k^6 + \mathrm{Ra}\,k_\perp^2}, \\ \frac{\tilde{\Theta}(\boldsymbol{k})}{8\pi} &= \frac{1}{k^2} - \frac{\mathrm{Ra}\,k_\perp^2}{k^2(k^6 + \mathrm{Ra}\,k_\perp^2)}, \end{aligned} \tag{43}$$

where we wrote the solution as the solution at zero Rayleigh number and the correction due to finite Ra. The Green function G_{ik} at $\mathrm{Ra} = 0$ is the Oseen tensor G^0_{ik} that obeys $G^0_{ik}(\boldsymbol{k})/(8\pi) = \Pi_{ik}(\boldsymbol{k})/k^2$; see, e.g., [12]. Similarly, the Fourier transform k^{-2} of the fundamental solution of the Laplace equation determines $\tilde{\Theta}(\boldsymbol{k})$ at $\mathrm{Ra} = 0$. There is no need for a separate consideration of $\boldsymbol{\Theta}$ because that is given by the reciprocal relation $\Theta_i(\boldsymbol{x}) = -\tilde{G}_i(-\boldsymbol{x})/\mathrm{Ra}$. We find by considering the inverse Fourier transform that the components of the Green function have a self-similar scaling dependence on the Rayleigh number (which is obeyed also by the $\mathrm{Ra} = 0$ part of the solution):

$$\begin{aligned} G_{ik}(\boldsymbol{x}) &= \frac{\delta_{ik}}{x} + \frac{x_i x_k}{x^3} - \mathrm{Ra}^{1/4} G'_{ik}(\mathrm{Ra}^{1/4}\boldsymbol{x}), \quad \tilde{G}_i(\boldsymbol{x}) = \mathrm{Ra}^{3/4}\tilde{G}'_i(\mathrm{Ra}^{1/4}\boldsymbol{x}), \\ \tilde{\Theta}(\boldsymbol{x}) &= \frac{2}{x} - \mathrm{Ra}^{1/4}\tilde{\Theta}'(\mathrm{Ra}^{1/4}\boldsymbol{x}), \end{aligned} \tag{44}$$

where we introduced

$$\begin{aligned} G'_{ik}(\boldsymbol{x}) &= \int \frac{\Pi_{iz}(\boldsymbol{q})\Pi_{zk}(\boldsymbol{q})}{q^6 + q_\perp^2}\frac{\exp(i\boldsymbol{q}\cdot\boldsymbol{x})d\boldsymbol{q}}{\pi^2}, \quad \tilde{G}'_i(\boldsymbol{x}) = \int \frac{q^2\Pi_{iz}(\boldsymbol{q})}{q^6 + q_\perp^2}\frac{\exp(i\boldsymbol{q}\cdot\boldsymbol{x})d\boldsymbol{q}}{\pi^2}, \\ \tilde{\Theta}'(\boldsymbol{x}) &= \int \frac{q_\perp^2}{q^2(q^6 + q_\perp^2)}\frac{\exp(i\boldsymbol{q}\cdot\boldsymbol{x})d\boldsymbol{q}}{\pi^2}, \end{aligned} \tag{45}$$

with $\boldsymbol{k} = \mathrm{Ra}^{1/4}\boldsymbol{q}$. The asymptotic series for the solution at distances from the source much smaller than the Rayleigh scale, $\mathrm{Ra}^{1/4}x \ll 1$, is obtained by the Taylor expansion of $G'_{ik}(\boldsymbol{x})$, $\tilde{G}'_i(\boldsymbol{x})$ and $\tilde{\Theta}'(\boldsymbol{x})$

at $x = 0$. Calculations performed in Sec. V of the Supplemental Material [42] give

$$G_{ik}(\boldsymbol{x}) = \frac{\delta_{ik}}{x} + \frac{x_i x_k}{x^3} - \mathrm{Ra}^{1/4}\lambda_i\delta_{ik} - \frac{\mathrm{Ra}^{3/4}}{2}x_l x_r \frac{\partial^2 G'_{ik}}{\partial x_l \partial x_r}(\boldsymbol{x} = 0) + O(\mathrm{Ra}^{5/4}x^4), \tag{46}$$

where the coefficients can be written with the help of the beta function $B(x, y)$ as

$$\lambda_z = 8B\left(\frac{9}{4}, \frac{9}{4}\right), \quad \lambda_{x,y} = \frac{1}{2\sqrt{2}}B\left(\frac{5}{4}, \frac{3}{2}\right), \quad \nabla^2 G'_{zz}(0) = -16B\left(\frac{11}{4}, \frac{11}{4}\right),$$
$$\nabla^2 G'_{xx,yy}(0) = -\frac{1}{2\sqrt{2}}B\left(\frac{7}{4}, \frac{3}{2}\right). \tag{47}$$

We see that the leading-order correction to the Oseen tensor for $G_{ik}(\boldsymbol{x})$ is a constant diagonal matrix [7,10]. The higher-order correction provided here is needed for the calculation of the drag in the next section, for which we need only the coefficients of the diagonal matrix $\nabla^2 G_{ik}(0)$. We have for the other components of the fundamental solution:

$$\tilde{G}_i(\boldsymbol{x}) = 4\mathrm{Ra}^{3/4}\delta_{iz}B\left(\frac{7}{4}, \frac{7}{4}\right) + O(\mathrm{Ra}^{5/4}x^2), \quad \tilde{\Theta}(\boldsymbol{x}) = \frac{2}{x} - 2\mathrm{Ra}^{1/4}B\left(\frac{5}{4}, \frac{5}{4}\right) + O\left(\mathrm{Ra}^{3/4}x^2\right), \tag{48}$$

with the corresponding expansion for $\Theta_i(\boldsymbol{x}) = -\tilde{G}_i(-\boldsymbol{x})/\mathrm{Ra}$; see details in Sec. V of the Supplemental Material [42].

In the case we are interested in, the particle moves vertically, and the $\boldsymbol{g}$ relevant for the flow description in the later section is directed along the z axis. We can consider with no loss $\boldsymbol{g} = g\hat{z}$ in Eq. (32). The flow in this case is axisymmetric and can be derived from the stream function that in cylindrical coordinates (ρ, z) obeys

$$u'_z = \frac{1}{\rho}\frac{\partial\psi}{\partial\rho}, \quad u'_\rho = -\frac{1}{\rho}\frac{\partial\psi}{\partial z}, \quad \psi = \int_0^\rho \rho' u'_z(\rho', z)d\rho', \tag{49}$$

where $u'_\rho = (xu'_x + yu'_y)/\sqrt{x^2 + y^2}$. The derivation in Sec. VI of the Supplemental Material [42] yields

$$\psi = \frac{\rho}{\mathrm{Ra}^{3/4}}\frac{\partial}{\partial\rho}(g\nabla^2 - s\,\mathrm{Ra})I(\mathrm{Ra}^{1/4}\boldsymbol{r}), \quad I(\boldsymbol{x}) = \int \frac{\exp(i\boldsymbol{q}\cdot\boldsymbol{x})}{q^6 + q_\perp^2}\frac{d\boldsymbol{q}}{(2\pi)^3}. \tag{50}$$

This is a compact formula for the description of the axisymmetric component of the fundamental solution. Computed stream function distributions using the formula [Eq. (32) given in Section VI of Supplemental Material [42]] for $\mathrm{Ra} = 0.001, 0.01, 0.1$, and 1 are compared with the numerical solution around a finite-size sphere obtained at $\mathrm{Re} = 0.01$ and $\mathrm{Pr} = 0.72$ in Fig. 2. According to the far flow approximation given in Sec. VII of the Supplemental Material [42], $g = F$ (drag force of the corresponding flow) and $s = \pi v_z/6 = -\pi/6$ are adopted in the computation of the stream function. As Ra increases toward 1, the vertical motion tends to be constrained in both the fundamental and numerical solutions, and agreement between the two solutions becomes poor since the Rayleigh scale $\mathrm{Ra}^{-1/4}$ decreases toward 1. It is noted that although the Reynolds number is as low as 0.01 for the numerical solution, the up-down symmetry is a little broken.

D. Force

In this section, we derive the limiting form of the force on the particle at small Rayleigh numbers up to the order $\mathrm{Ra}^{5/4}$. The previous studies by [10] assumed a scale separation of $\mathrm{Ra}^{-1/4} \gg 1$, relying on matching of the Stokes flow around the particle that holds at $x \ll \mathrm{Ra}^{-1/4}$ with the far field Stokeslet approximation that holds at $x \gg 1$. The inequality $x \gg 1$ allowed the point force approximation of the particle to be used, and $x \ll \mathrm{Ra}^{-1/4}$ allowed the small argument asymptotic form of the Green function considered in the previous section to be used. The flow at $1 \ll x \ll \mathrm{Ra}^{-1/4}$ is the Stokes flow with a constant correction. This situation is similar to the classical Lorentz

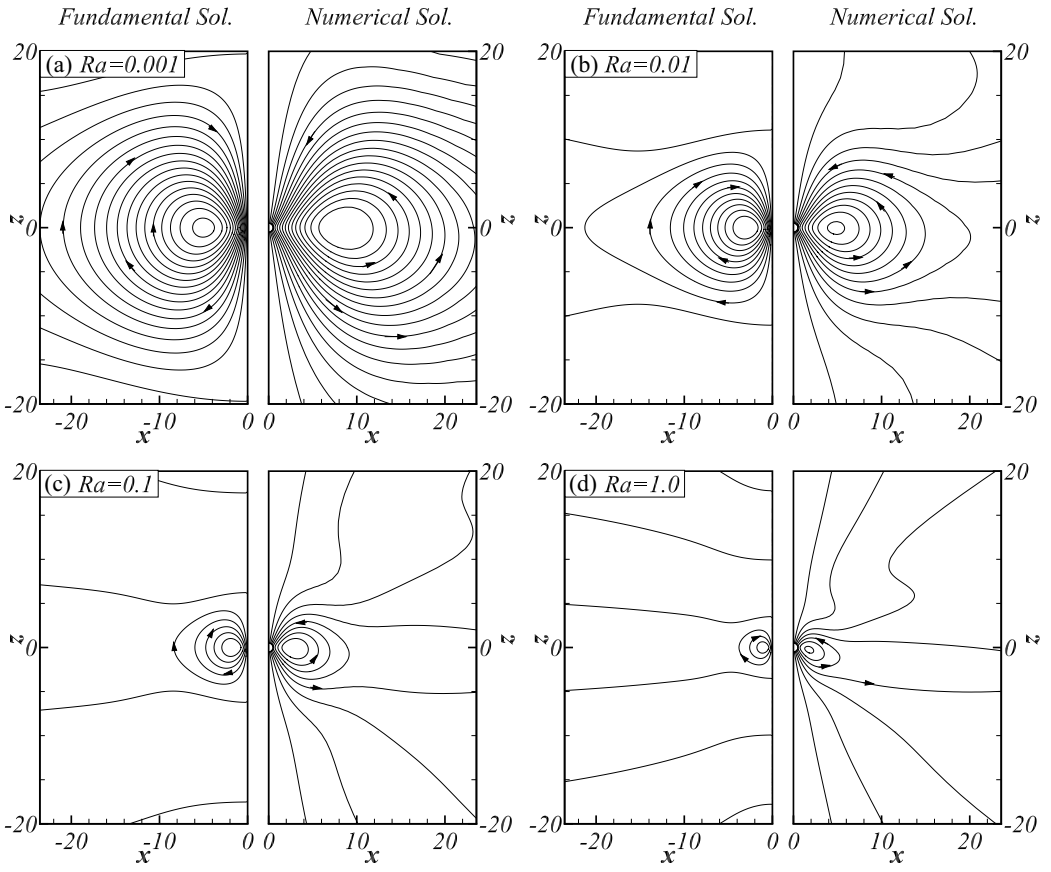

FIG. 2. Stream function distribution of the fundamental solution compared with numerical solution which was obtained for Re = 0.01 and Pr = 0.72.

treatment of the correction to the Stokes drag due to the far wall, where the flow induced by the image at the position of the particle is approximately constant [9]. There is a good reason for that: the stratification acts as an effective wall at a scale of order $\mathrm{Ra}^{-1/4}$ because the flow falls off rapidly beyond that scale. Thus, proceeding as in the wall problem, the correction to the Stokes drag is obtained [10]. It is, however, not so obvious how corrections to this procedure, and thus also the domain of its validity, could be derived: when $\mathrm{Ra}^{1/4} \sim 1$, the situation is similar to the transition from the case of the far wall to the case of the wall at a distance of order 1. Thus, we introduce here a different procedure that relies on the integral equation on the surface traction.

The force is determined by $\boldsymbol{u}_1$, which obeys the integral representation given by Eq. (36). We take in this representation the limit of $\boldsymbol{x}$ tending to the surface of the sphere. This limit is regular due to the regular behavior of $\tilde{G}_i$ at small distances; see Eq. (48). Using the boundary condition, we find the integral equation on the surface traction σ_{kr}:

$$-8\pi v_i = \int_{r=1/2} G_{ik}(\boldsymbol{x}-\boldsymbol{x}')\sigma_{kr}(\boldsymbol{x}')dS' - v_z \int_{r<1/2} \tilde{G}_i(\boldsymbol{x}-\boldsymbol{x}')d\boldsymbol{x}' - \int_{r=1/2} \theta(\boldsymbol{x}')\nabla'_r \tilde{G}_i(\boldsymbol{x}-\boldsymbol{x}')dS', \tag{51}$$

where we do not write the index of the solution in this section as we are working with $\boldsymbol{u}_1$ only. This equation must hold for all $\boldsymbol{x}$ on the sphere surface, and its solution determines σ_{kr}; see, e.g., [12].

Using Eq. (46), we have in the leading nontrivial order in Ra that

$$-8\pi\left(v_i-\frac{\mathrm{Ra}^{1/4}\lambda_i F_i}{8\pi}\right)=\int_{r=1/2}G^0_{ik}(\boldsymbol{x}-\boldsymbol{x}')\sigma_{kr}(\boldsymbol{x}')dS', \tag{52}$$

where there is no summation over the repeated indices. We found the equation on the surface traction for a particle that moves in an unstratified fluid with a velocity given by $v_i-\mathrm{Ra}^{1/4}M_{ii}F_i/(8\pi)$; cf. [12]. We conclude that the force and the surface traction obey

$$F_i=-3\pi\left(v_i-\frac{\mathrm{Ra}^{1/4}\lambda_i F_i}{8\pi}\right),\quad \sigma_{ir}(\boldsymbol{x})=\frac{F_i}{\pi}=-3\left(v_i-\frac{\mathrm{Ra}^{1/4}\lambda_i F_i}{8\pi}\right), \tag{53}$$

where 3π is the Stokes force F_{St} in our dimensionless variables, and we use the fact that the surface traction of the Stokes flow around the translating particle is uniform (the surface area is π). We find that

$$F_i=-3\pi v_i\left(1-\frac{3\mathrm{Ra}^{1/4}\lambda_i}{8}\right)^{-1}\approx -3\pi v_i\left(1+\frac{3\mathrm{Ra}^{1/4}\lambda_i}{8}\right). \tag{54}$$

We obtain, using the formulas for λ_i, that (we write F_{st} in the answer and not 3π since in this form the formula is also valid in dimensional variables)

$$F_z\approx F_{St}\left[1+3\mathrm{Ra}^{1/4}B\left(\frac{9}{4},\frac{9}{4}\right)\right];\quad F_{x,y}\approx F_{St}\left[1+\frac{3\mathrm{Ra}^{1/4}}{16\sqrt{2}}B\left(\frac{5}{4},\frac{3}{2}\right)\right], \tag{55}$$

where we also provide the answers for the case of horizontal motion beyond the considered sedimentation problem. These answers agree with [10]. We consider higher-order corrections using Eqs. (46)–(48):

$$\begin{aligned}-8\pi v_i=&\int_{r=1/2}G^0_{ik}(\boldsymbol{x}-\boldsymbol{x}')\sigma_{kr}(\boldsymbol{x}')dS'-\mathrm{Ra}^{1/4}\lambda_i F_i-\frac{\mathrm{Ra}^{3/4}}{2}\frac{\partial^2 G'_{ik}}{\partial x_l\partial x_r}(\boldsymbol{x}=0)\\&\times\int_{r=1/2}(\boldsymbol{x}-\boldsymbol{x}')_l(\boldsymbol{x}-\boldsymbol{x}')_r\sigma_{kr}(\boldsymbol{x}')dS'-\frac{2\pi v_z\mathrm{Ra}^{3/4}\delta_{iz}}{3}B\left(\frac{7}{4},\frac{7}{4}\right).\end{aligned} \tag{56}$$

In the last term on the right-hand side of the first line, we can take for the surface traction $\sigma_{kr}(\boldsymbol{x}')$ its value $-3v_k$ at $\mathrm{Ra}=0$; see Eq. (53). We observe that

$$\int_{r=1/2}(\boldsymbol{x}-\boldsymbol{x}')_l(\boldsymbol{x}-\boldsymbol{x}')_r dS'=\pi x_l x_r+\frac{\pi\delta_{lr}}{12}, \tag{57}$$

where we used $\int_{r=1/2}x'_l x'_r dS'=\pi\delta_{lr}/12$. We conclude that in the considered order the surface traction obeys

$$\begin{aligned}&-8\pi\left[v_i-\frac{\mathrm{Ra}^{1/4}\lambda_i F_i}{8\pi}-\frac{v_z\mathrm{Ra}^{3/4}\delta_{iz}}{12}B\left(\frac{7}{4},\frac{7}{4}\right)+\frac{3v_k\mathrm{Ra}^{3/4}}{16}\frac{\partial^2 G'_{ik}(0)}{\partial x_l\partial x_r}x_l x_r+\frac{v_k\mathrm{Ra}^{3/4}}{64}\frac{\partial^2 G'_{ik}(0)}{\partial x_l\partial x_l}\right]\\&=\int_{r=1/2}G^0_{ik}(\boldsymbol{x}-\boldsymbol{x}')\sigma_{kr}(\boldsymbol{x}')dS'.\end{aligned} \tag{58}$$

This is the equation on the surface traction of a particle that moves in an unstratified flow with a nontrivial velocity distribution on the surface given by the coefficient of -8π in the first line. The force is the superposition of the Stokes force $\boldsymbol{F}'_0$, determined by the coordinate-independent component of the velocity distribution, and the force $\boldsymbol{F}_0$ caused by the term proportional to $x_l x_r$. The force component $\boldsymbol{F}_0$ can be found using the standard reciprocal theorem for the Stokes flows, see, e.g., [9,12]. Applying the theorem for the Stokes flow with velocity $\boldsymbol{V}$ and the flow determined

by the boundary condition's term proportional to $x_l x_r$ gives

$$\boldsymbol{V}\cdot\boldsymbol{F}_0 = -V_i\frac{9v_k\mathrm{Ra}^{3/4}}{16}\frac{\partial^2 G'_{ik}(0)}{\partial x_l\partial x_r}\int_{r=1/2} x_l x_r dS = -V_i\frac{3\pi v_k\mathrm{Ra}^{3/4}}{64}\frac{\partial^2 G'_{ik}(0)}{\partial x_l\partial x_l}, \tag{59}$$

where we used the surface traction of the Stokes flow, $-3\boldsymbol{V}$. We conclude that F_{0i} is the coefficient of V_i in the last term. We find summing $\boldsymbol{F}'_0$ and $\boldsymbol{F}_0$,

$$F_i = -3\pi\left[v_i - \frac{\mathrm{Ra}^{1/4}\lambda_i F_i}{8\pi} - \frac{v_z\mathrm{Ra}^{3/4}\delta_{iz}}{12}B\left(\frac{7}{4},\frac{7}{4}\right) + \frac{v_k\mathrm{Ra}^{3/4}}{64}\frac{\partial^2 G'_{ik}(0)}{\partial x_l\partial x_l}\right] - \frac{3\pi v_k\mathrm{Ra}^{3/4}}{64}\frac{\partial^2 G'_{ik}(0)}{\partial x_l\partial x_l},$$

where $\nabla^2 G'_{ik}(0)$ is the diagonal matrix; see Sec. V of the Supplemental Material [42]. Solving with respect to F_i gives

$$F_i = F_{St}\left[1-\frac{3\mathrm{Ra}^{1/4}\lambda_i}{8}\right]^{-1}\left[1-\frac{\mathrm{Ra}^{3/4}\delta_{iz}}{12}B\left(\frac{7}{4},\frac{7}{4}\right)+\frac{\mathrm{Ra}^{3/4}}{32}\frac{\partial^2 G'_{ii}(0)}{\partial x_l\partial x_l}\right], \tag{60}$$

or in components

$$\begin{aligned}\frac{F_z}{F_{St}} &= \left[1-3\mathrm{Ra}^{1/4}B\left(\frac{9}{4},\frac{9}{4}\right)\right]^{-1}\left[1-\frac{\mathrm{Ra}^{3/4}}{12}B\left(\frac{7}{4},\frac{7}{4}\right)-\frac{\mathrm{Ra}^{3/4}}{2}B\left(\frac{11}{4},\frac{11}{4}\right)\right],\\ \frac{F_{x,y}}{F_{St}} &= \left[1-\frac{3\mathrm{Ra}^{1/4}}{16\sqrt{2}}B\left(\frac{5}{4},\frac{3}{2}\right)\right]^{-1}\left[1-\frac{\mathrm{Ra}^{3/4}}{64\sqrt{2}}B\left(\frac{7}{4},\frac{3}{2}\right)\right],\end{aligned} \tag{61}$$

with the corresponding formula for $F_{x,y}$. The corrections to these formulas are of order $\mathrm{Ra}^{5/4}$; therefore, the formulas apply at $\mathrm{Ra}^{5/4}\ll 1$, which is a much less stringent condition than $\mathrm{Ra}^{1/4}\ll 1$ in [10]. The difference from the formulas of [10] would be large when $\mathrm{Ra}^{3/4}\sim 1$ in the range of applicability $\mathrm{Ra}^{5/4}\ll 1$. Later, this formula for the corrected drag of the sedimenting sphere, which is one of our main results, will be compared with the numerical estimation as well as with the prediction by [10].

Finally, the integral representations given by Eqs. (36) and (37) can be used in the standard way [12,13] to derive the multipole expansion of the solution that describes the flow at large distances from the particle. Similarly to unstratified flow, this term is determined by a point force approximation with the force that was studied in the previous section. However, the particle also produces a source in the heat equation whose contribution to the flow is of comparable magnitude with the point force contribution at $\mathrm{Ra}^{3/4}\gtrsim 1$. This term was disregarded in previous studies. A detailed derivation of the far field flow is provided in Sec. VII of the Supplemental Material [42].

IV. NUMERICAL RESULTS

In the previous section, we obtained an analytic solution of the stratified flow around a sedimenting sphere in the small-Reynolds-number and small-Rayleigh-number limits, which is valid only for the Stokes flow regime. In this section, we numerically investigate the same problem for finite Reynolds and Rayleigh numbers solving the full equations [Eq. (4)] in the moving frame using the numerical method explained in Sec. II B. The considered parameter ranges are $0.005\leqslant\mathrm{Re}\leqslant 10$ and $10^{-4}\leqslant\mathrm{Ra}\leqslant 1.5$ for the three values $\mathrm{Pr}=0.72$, 7.0, and 700 corresponding to air, water, and seawater, respectively. The numerical results of drag modification for the smallest Re will be compared with the analytic prediction.

A. Drag modification

Figures 3 and 4 show the drag enhancement normalized by the drag of unstratified flow computed from our simulations for $\mathrm{Pr}=0.72$, 7, and 700 in the linear-linear scale and the log-log

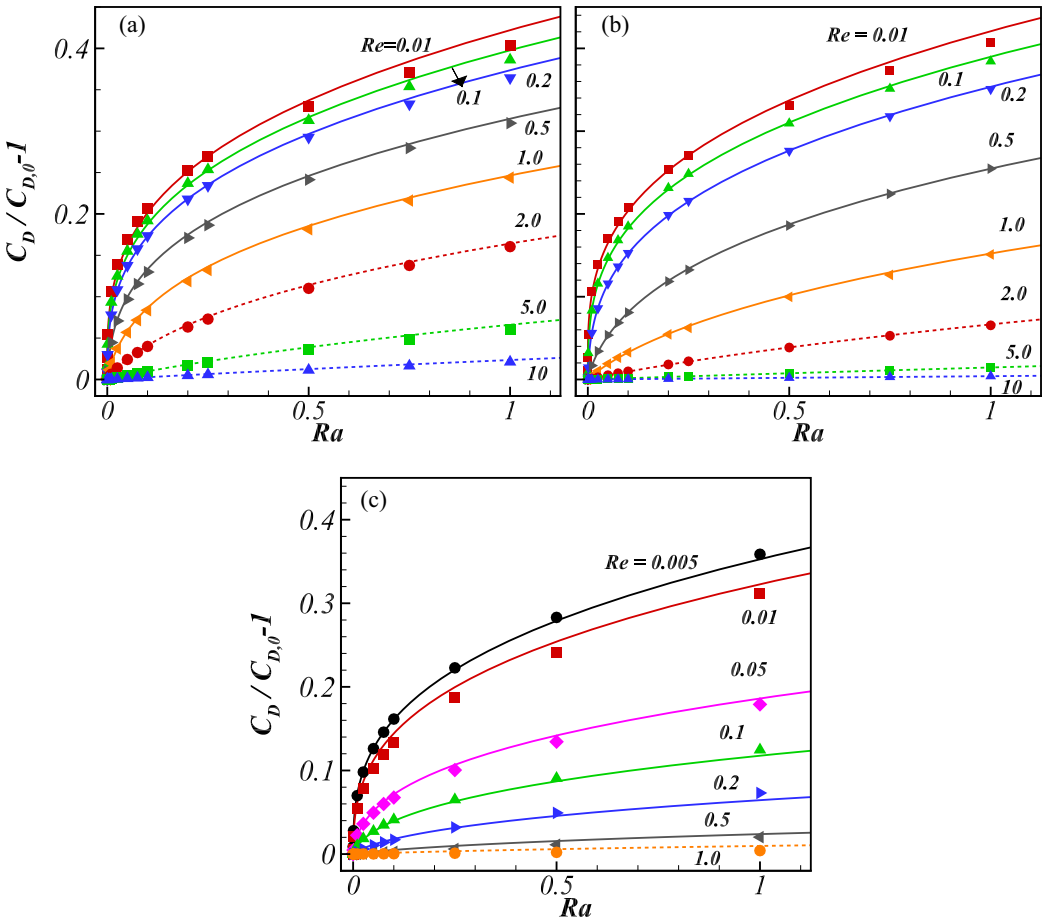

FIG. 3. Enhanced drag normalized by the drag of unstratified flow as a function of Ra and Re for (a) Pr = 0.72, (b) 7, and (c) 700 in linear-linear scale. Symbols denote computed data, and lines represent the fitting equation, Eq. (62).

scale, respectively, for the ranges of Re = 0.005 ∼ 10 and Ra = 10^{-4} ∼ 1.5. When Re = 0.01, stratification increases the drag of a sedimenting sphere by up to 40% at Ra = 1, equally for Prandtl numbers 0.72 and 7. However, even when Re = 0.005, the drag enhancement at Ra = 1 for Prandtl number 700 is about 35%. As the Reynolds number increases, the effect of stratification becomes weaker. For example, when Re = 10, the drag is hardly modified by stratification for Pr = 0.72 and 7. For Pr = 700, the drag is not influenced by stratification when Re = 1. It can be seen from the log-log plot of the drag enhancement that when the Reynolds number is low, the drag enhancement increases with the Rayleigh number as ∼Ra^{α}, with $\alpha = 1/4 \sim 1/3$, while it increases linearly with the Rayleigh number for high Reynolds numbers. α tends to 1/3 as the Rayleigh number increases. From these observations, we provide a new formula for the drag enhancement:

$$\frac{C_D}{C_{D,0}} = 1 + \frac{\mathrm{Ra}}{a + b\mathrm{Ra}^{1/3} + c\mathrm{Ra}^{2/3}}, \quad \text{for Ra} \leqslant 1.5, \quad \mathrm{Re} \leqslant 10, \tag{62}$$

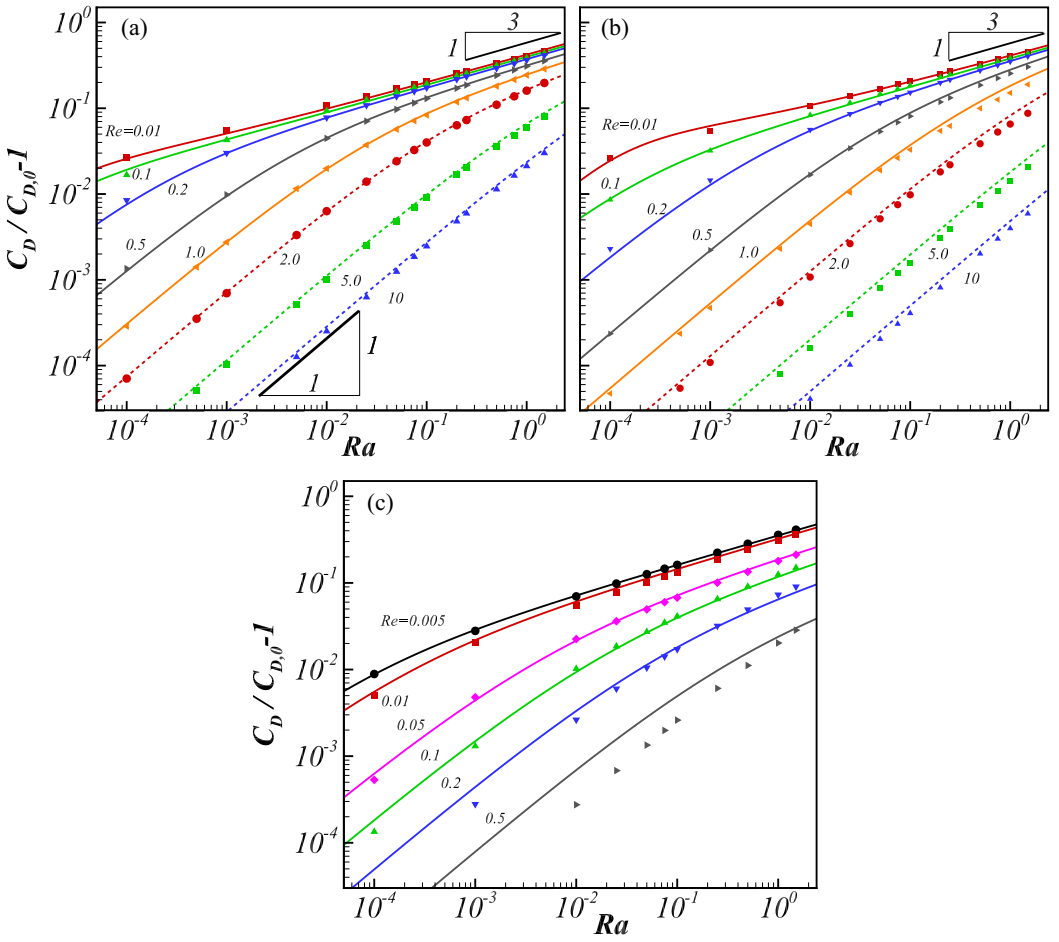

FIG. 4. Enhanced drag normalized by the drag of unstratified flow as a function of Ra and Re for (a) Pr = 0.72, (b) 7, and (c) 700 in log-log scale. The lines represent Eq. (62). The solid symbols denote computed data.

where $C_{D,0}$ is the drag coefficient for the unstratified case for all Reynolds numbers, small or finite, and a, b, and c are the functions of Pr and Re:

$$\mathrm{Pr} = 0.72: \begin{cases} a = 0.017\,97 - 0.037\,28\,\mathrm{Re} + 0.348\,22\,\mathrm{Re}^2 \\ b = -0.063\,29 + 0.214\,78\,\mathrm{Re} + 0.956\,46\,\mathrm{Re}^2 \\ c = 2.414\,16 + 3.9022(1 - \exp^{(-0.3594\,\mathrm{Re})}) \end{cases}, \tag{63}$$

$$\mathrm{Pr} = 7: \begin{cases} a = 0.007\,52 - 0.020\,49\,\mathrm{Re} + 2.009\,36\,\mathrm{Re}^2 \\ b = -0.211\,54 + 0.561\,02\,\mathrm{Re} + 0.493\,02\,\mathrm{Re}^2 \\ c = 2.569\,21 + 4.6469(1 - \exp^{(-0.179\,07\,\mathrm{Re})}) \end{cases}, \tag{64}$$

$$\mathrm{Pr} = 700: \begin{cases} a = 0.002\,51 - 0.083\,24\,\mathrm{Re} + 46.2\,\mathrm{Re}^2 \\ b = -0.013\,121 + 19.696\,13\,\mathrm{Re} + 1.167\,95\,\mathrm{Re}^2 \\ c = 2.594\,08 + 104.528\,88(1 - \exp^{(-0.400\,65\,\mathrm{Re})}) \end{cases}. \tag{65}$$

This equation [Eq. (62)] fits the computed data very well, as shown in Figs. 3 and 4.

Now we test our theoretical prediction of drag enhancement against the numerical result for low Reynolds numbers. Candelier *et al.* [10] derived the following correction of the drag under the

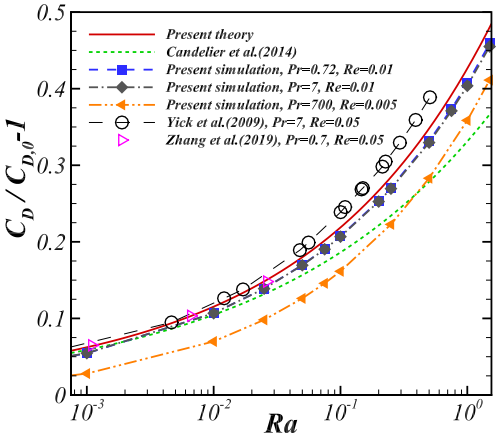

FIG. 5. Drag enhancement as a function of Rayleigh number Ra for Prandtl numbers 0.72 and 7 at Re = 0.01 compared with our theoretical prediction, Eqs. (67) and (66) from [10] in log-linear scales. The case for Pr = 700 and Re = 0.005 is also presented for comparison. Simulation data by Yick *et al.* [11] and Zhang *et al.* [38] are included as well.

Stokes flow assumption:

$$\frac{C_D}{C_{D,0}} = 1 + 0.3311\,\mathrm{Ra}^{1/4}, \tag{66}$$

where $C_{D,0}$ is the Stokes drag coefficient in an unstratified medium, while our prediction with higher-order corrections is obtained from Eq. (61) after evaluating the β function:

$$\begin{aligned}\frac{C_D}{C_{D,0}} &= (1 - 0.3311\,\mathrm{Ra}^{-1/4})^{-1} \times (1 - 0.045\,89\,\mathrm{Ra}^{3/4})\text{or}\\ &= 1 + 0.3311\,\mathrm{Ra}^{1/4} + 0.1096\,\mathrm{Ra}^{1/2} - 0.009\,60\,\mathrm{Ra}^{3/4}.\end{aligned} \tag{67}$$

We can immediately see that our higher-order terms are not negligible near an order-1 Rayleigh number. Figure 5 shows the drag enhancement as a function of the Rayleigh number Ra at Re = 0.01 for Prandtl numbers 0.72 and 7 compared with our theoretical prediction, Eqs. (67) and (66) from [10] in log-linear scales. The drag enhancement for both Prandtl numbers collapses very well at this Reynolds number, as predicted by small Reynolds and Péclet number limits. However, the drag enhancement for Pr = 700 and Re = 0.005 shows deviation from our theoretical prediction and Candelier's prediction because even for the smallest Reynolds number of 0.005, the Péclet number becomes 3.5, which violates the small Péclet number condition Pe $\ll 1$ for theory. It also indicates that the effect of inertia suppresses the stratification effect in enhancing drag. Our theoretical prediction, Eq. (67), clearly matches numerical data better than Eq. (66) for the range Ra > 0.05, confirming that the higher-order corrections are indeed not negligible. The simulation of Yick *et al.* [11] slightly overpredicts the enhancement, possibly due to their insufficient domain size ($80d \times 40d$ compared to our domain size of $300d \times 300d$). Recent simulation by Zhang *et al.* [38] clearly matches our theoretical prediction better than Candelier's prediction, although differences are small.

Enhanced drag by stratification obviously indicates retardation of the settling motion of particles. We consider as an example the settling velocity of a Volvox for the typical value of the Rayleigh scale $L = 1$ mm [8]. The density offset $\rho_p/\rho_f - 1$ depends on the micro-organism's radius, since Volvox becomes more hollow at increasing size. The data of [40], for most points (the density offset is not a unique function of size due to biological diversity), can be fit by the linear law for density

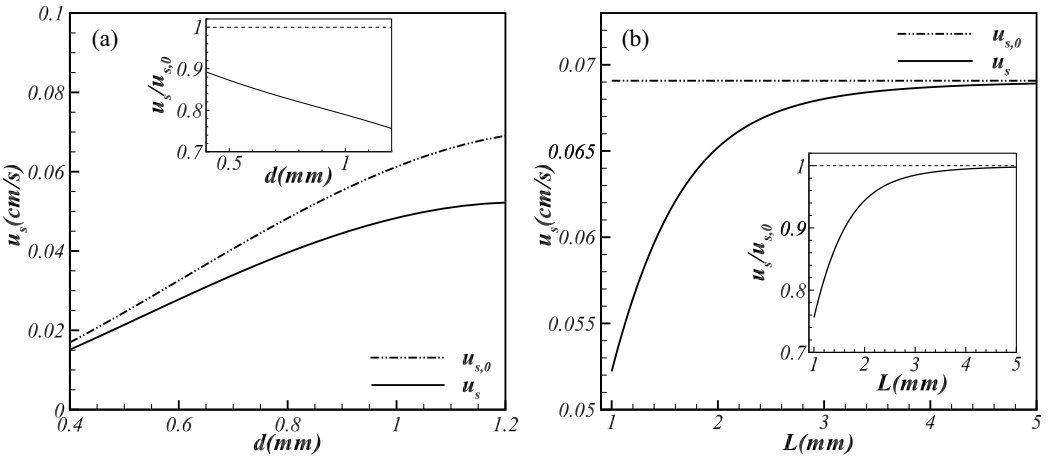

FIG. 6. Settling velocity of Volvox u_s (solid line) whose diameter is d in stratified fluid at rest as compared with that in unstratified fluid $u_{s,0}$ (dash-dot-dot line). (a) u_s as a function of diameter at a fixed Rayleigh scale $L = 1$ mm. (b) u_s of a Volvox with diameter $d = 1.2$ mm as a function of the Rayleigh scale. The inset shows the ratio $u_s/u_{s,0}$.

offset as a function of diameter d (mm): $\rho_p/\rho_f - 1 = 0.001 \times [2 - (d - 0.4)/0.8]$. It is found that the settling velocity in a stratified fluid at rest decreases by as much as 25% as compared with that in an unstratified fluid, see Fig. 6(a). For a Volvox of diameter $d = 1.2$ mm, the settling velocity as a function of the Rayleigh scale is also given in Fig. 6(b). As the stratification intensifies (or, L decreases toward the scale of the Volvox), the settling velocity decreases rapidly. Here, the settling velocity u_s is determined from

$$C_D \frac{1}{2}\rho_f u_s^2 \frac{\pi d^2}{4} - (\rho_p - \rho_f) g \frac{4\pi}{3}\left(\frac{d}{2}\right)^3 = 0, \tag{68}$$

where $C_D/C_{D,0}$ is given by Eq. (62) for $\mathrm{Pr} = 7$, and the drag coefficient in an unstratified fluid $C_{D,0}$ is calculated by [43]

$$C_{D,0} = \frac{24}{\mathrm{Re}_p}\left(1 + 0.15\,\mathrm{Re}_p^{0.687}\right), \tag{69}$$

with $\mathrm{Re}_p = u_s d/\nu$.

B. Flow characteristics

The effect of Ra and Re on the modification of the streamlines in the absolute frame of reference and the normalized temperature distribution is demonstrated in Fig. 7 at $\mathrm{Pr} = 7$. When the Reynolds number is low ($\mathrm{Re} = 0.1$), compared with the streamlines in an unstratified medium, which are close to those of Stokes flow, the streamlines of the flow for finite Rayleigh numbers ($\mathrm{Ra} = 0.001, 0.1$) retain the fore-and-apt symmetry but tend to close near the sphere due to suppression of the vertical motion. The center of the closed streamlines is found to be approximately horizontally cL off from the center of the sphere with $c \sim 2$. As the Reynolds number increases, the flow loses symmetry and the effect of stratification becomes weaker because the nonlinear advection dominates the buoyancy as well as the diffusion process. Despite the drastic change in the streamlines at low Reynolds numbers, the temperature distribution is hardly modified by the stratification strength. Deflection from the vertically increasing distribution of temperature is noticeable only when the Reynolds number is not small. Although we have not shown the streamlines for $\mathrm{Pr} = 0.72$ and the temperature

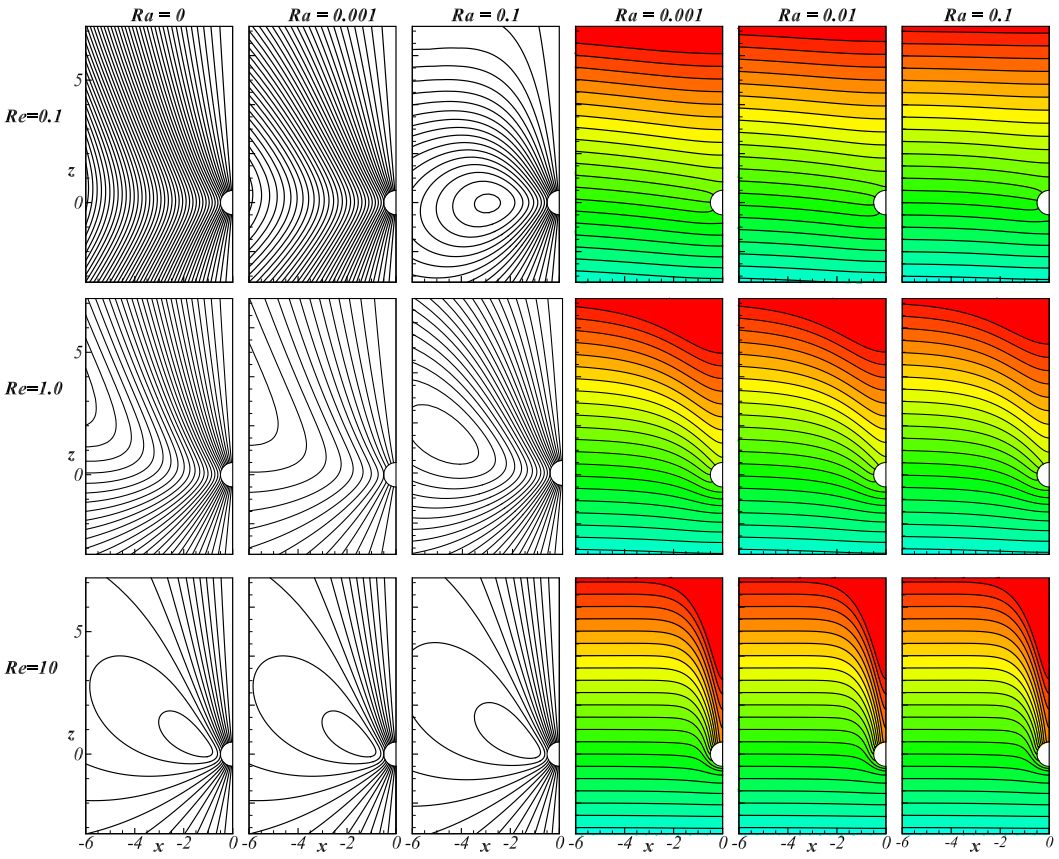

FIG. 7. Modification of streamlines and dimensionless temperature field in the wake of a settling sphere due to the stratification and Reynolds number at Pr = 7 (Ra = 10^{-3}, 10^{-2}, and 10^{-1} and Re = 0.1, 1.0, and 10).

distribution, the streamline pattern is similar, while the normalized temperature distribution exhibits less deviation from the horizontally uniform distribution.

Finally, Fig. 8 demonstrates the magnitude of the vertical velocity u_z normalized by the nondimensional Rayleigh scale L/d (=$\mathrm{Ra}^{-1/4}$) along the normalized distance in both axes (a) x and (b) z. The lines represent the value of the vertical velocity for Pr = 0.72, and the symbols represent those of the Pr = 7 case. Along the horizontal x axis, the normalized vertical velocity for both Prandtl numbers and all Rayleigh numbers considered collapses to one line. One local minimum point is found at $\mathrm{Ra}^{1/4}x \approx 3$, indicating a sign change. The decaying behavior with a constant rate of -1, similar to that of the Stokeslet [7], is observed for $\mathrm{Ra}^{1/4}x \leqslant 1$ or $x \leqslant L/d$.

Along the vertical z axis, the vertical velocity for both Prandtl numbers shows oscillatory decaying behavior for all the Rayleigh numbers considered. For the Pr = 7 case, all local minimum points for every Rayleigh number collapse well. However, the local minimum point does not match between the two Prandtl number cases. As with the distribution along the horizontal direction, a good collapse with a decay rate of 1 is observed for $\mathrm{Ra}^{1/4}z \leqslant 1$ or $z \leqslant L/d$, and the velocity decays faster for $z > L/d$.

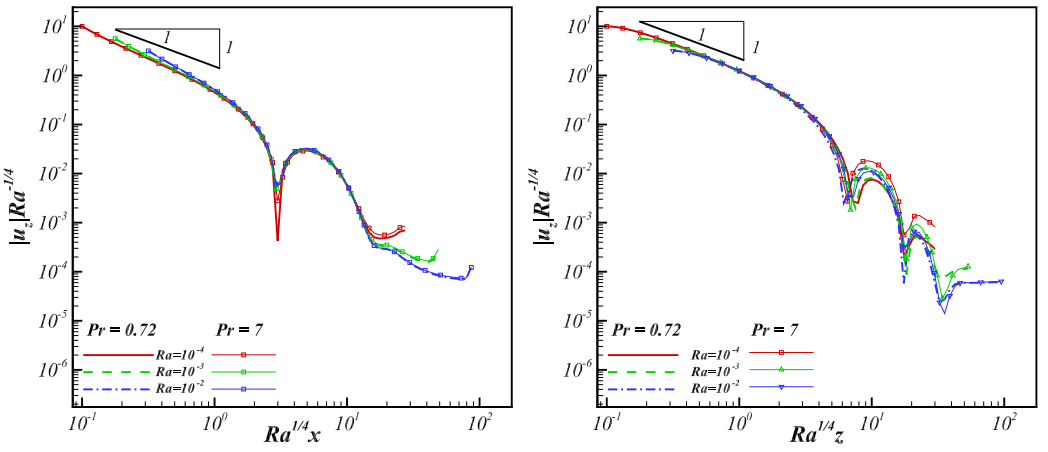

FIG. 8. Normalized vertical velocity $|u_z|\mathrm{Ra}^{-1/4}$ along (a) the horizontal axis x and (b) the vertical axis z for $\mathrm{Pr} = 0.72$ and 7.

V. CONCLUSIONS

In this paper, we conducted an extensive study of the sedimentation of small particles in a stratified fluid. Our main theoretical result is the formula for the drag force at small Reynolds and Péclet numbers that holds under the condition $\mathrm{Ra}^{5/4} \ll 1$. This significantly increases the range of validity of previous studies, which was limited to $\mathrm{Ra}^{1/4} \ll 1$. Other results include the derivation of an integral representation of the flow, reciprocal relations and a modified Lorentz identity, and a full fundamental solution with a heat source and a description of the previously disregarded insulating component of the flow. So as not to overwhelm the text with details, we put the derivation of the far field form of the flow in the last section of the Supplemental Material [42]. That form demonstrates that the sedimenting insulating particle looks at large distances as both the point force and the point source of heat. The far field coincides with

$$\nabla p_1 = \mathrm{Ra}\,\theta_1\hat{z} + \nabla^2\boldsymbol{u}_1 - \boldsymbol{F}\delta(\boldsymbol{x}), \quad u_{1z} = \nabla^2\theta_1 + \frac{\pi v_z \delta(\boldsymbol{x})}{6}. \tag{70}$$

In contrast, with previous approaches the force $\boldsymbol{F}$ can be significantly different from the Stokes force in unstratified fluid and there is a heat source term in the last equation. The adiabatic surface changes the temperature distribution around the particle, and at large distances this change "looks" as if there is a heat source (or sink) at the particle's position. The amplitude of the source of heat is proportional to the velocity of the sedimenting particle, which depends on Ra nontrivially for stationary sedimentation. The heat source is negligible at $\mathrm{Ra}^{1/2} \ll 1$; however, at $\mathrm{Ra}^{1/2} \sim 1$, covered by the present theory also, this term theoretically must give an order-1 contribution in the far flow, see the details in the Supplemental Material [42]. We find, however, that the numerical factors cause this term not to make any noticeable difference in the far flow even for $\mathrm{Ra} = 1$.

We briefly consider the possibility of observing the insulating flow whose characteristic value is $\kappa\mathrm{Ra}/d$. We have, assuming $L = 1$ mm and $\kappa \sim 10^{-6}$ m^2/s (corresponding to a Prandtl number of order 1), that particles with a size of order 1 mm induce a flow of approximately 1 mm/s. This flow extends over a spatial scale of 1 mm ($d \sim L$) and displaces a nearby tracer by 1 mm in 1 s. This seems to be an observable phenomenon.

Our theoretical approach uses integral representation of the flow and finds the force directly, circumventing the study of the spatial structure of the flow. This is the key to the efficiency of this approach, which is well suited for the regime where the nonlinear terms in the fluid mechanical equations are negligible. The approach can be extended to include the time-derivative unsteady

term in the equations [12]. The inclusion of the nonlinear terms in the equations demands other approaches, such as the matched asymptotic expansions [6,37]. These approaches so far took the Stokes flow around particle moving in fluid at rest as the zero-order approximation. It is of interest to see if the calculations can also be done starting from a finite-Reynolds-number flow as the zero-order approximation.

We performed a detailed numerical study of the flow at Reynolds numbers smaller than 10 and Rayleigh numbers smaller than 1 using an FDMPM-1P. This allowed us to investigate the flow structures and temperature around the sphere. We considered two values of Prandtl number, 0.72 and 7. The results showed that the flow depends on the Reynolds, Rayleigh, and Prandtl numbers. The modified flow by the particle in a stably stratified fluid inhibits the vertical motion of the flow. The enhancement of the drag coefficient linearly increases with Ra for very low Ra and increases with the $1/3$ power of Ra for large Ra. We derived a fitting formula that captures the numerical results describing the drag over the whole range of the considered Reynolds and Rayleigh numbers. The vertical velocity (u_z) normalized by the length scale ratio $d/L(=\mathrm{Ra}^{1/4})$ along the normalized distance for both horizontal and vertical directions collapses on one line for $x \leqslant L/d$ and $z \leqslant L/d$.

Our results are ready for application to plankton and marine snow particles and can become a relevant tool in the study of the motion of these particles, which play a key role in the oceanic carbon cycle. It is estimated that the settling velocity of Volvox with $d = 1.2$ mm in stratified fluid with $L = 0.5$ mm is twice smaller than that in unstratified fluid. A particle that sediments in the presence of stratification would drag with it small tracer particles located on the closed streamlines of the flow. Thus, stratification brings about the qualitative effect of possible mass drag by sedimenting particles, an effect that does not exist for the open streamlines of Stokes flow in the unstratified case.

Finally, the effect of the presence of turbulence on the settling velocity of sedimenting particles is negligible as long as the turbulence is weak, and therefore the linear drag law produces almost the same settling velocity as that in the fluid at rest. However, when the turbulence is strong, the perturbed temperature gradient due to the turbulence could produce a nonlinear effect. The nondimensional parameter called the Cox number, defined as $\mathrm{Co} = \langle(\nabla T')^2\rangle/\gamma^2$, which measures such effects, can be as large as 290 in the ocean [44], and this clearly amplifies the local Rayleigh number. Strong turbulence can also cause a preferential concentration of particles that might modify the mean settling velocity of particles in stratified flow. Indeed, in the limit of small particle inertia a Maxey-type formula can be developed [45], giving the particle's velocity as the local incompressible turbulent flow plus a space-dependent correction due to a finite space-dependent Rayleigh number. This formula implies multifractal steady-state distribution of the particles; see, e.g., [46]. The consistent study of the behavior of the sedimenting particles in stratified turbulence could be performed in the future.

ACKNOWLEDGMENT

This research was supported by ADD (No. 17-113-601-026).

[1] L. P. Wang and M. R. Maxey, Settling velocity and concentration distribution of heavy particles in homogeneous isotropic turbulence, J. Fluid Mech. **256**, 27 (1993).

[2] A. L. Shanks and J. D. Trent, Marine snow: Sinking rates and potential role in vertical flux, Deep Sea Res. Part A **27**, 137 (1980).

[3] S. A. MacIntyre, L. Alldredge, and C. C. Gotschalk, Accumulation of marine snow at density discontinuities in the water column, Limnol. Oceanogr. **40**, 449 (1995).

[4] E. J. List, Laminar momentum jets in a stratified fluid, J. Fluid Mech. **45**, 561 (1971).

[5] A. M. Ardekani and R. Stocker, Stratlets: Low Reynolds Number Point-Force Solutions in a Stratified Fluid, Phys. Rev. Lett. **105**, 084502 (2010).
[6] Y. Zvirin and R. S. Chadwick, Settling of an axially symmetric body in a viscous stratified fluid, Int. J. Multiphase Flow **1**, 743 (1975).
[7] I. Fouxon and A. Leshansky, Convective stability of turbulent Boussinesq flow in the dissipative range and flow around small particles, Phys. Rev. E **90**, 053002 (2014).
[8] A. Doostmohammadi, R. Stocker, and A. M. Ardekani, Low-Reynolds-number swimming at pycnoclines, Proc. Natl. Acad. Sci. **109**, 3856 (2012).
[9] J. Happel and H. Brenner, *Low Reynolds Number Hydrodynamics: With Special Applications to Particulate Media* (Springer Science & Business Media, New York, 2012), Vol. 1.
[10] F. Candelier, R. Mehaddi, and O. Vauquelin, The history force on a small particle in a linearly stratified fluid, J. Fluid Mech. **749**, 184 (2014).
[11] K. Y. Yick, C. R. Torres, T. Peacock, and R. Stocker, Enhanced drag of a sphere settling in a stratified fluid at small Reynolds numbers, J. Fluid Mech. **632**, 49 (2009).
[12] S. Kim and S. J. Karrila, *Microhydrodynamics: Principles and Selected Applications* (Courier Corporation, North Chelmsford, MA, 2013).
[13] C. Pozrikidis, *Boundary Integral and Singularity Methods for Linearized Viscous Flow* (Cambridge University Press, Cambridge, England, 1992).
[14] P. S. Epstein, Zur theorie des radiometers, Z. Phys. **54**, 537 (1929).
[15] H. Brenner and J. R. Bielenberg, A continuum approach to phoretic motions: Thermophoresis, Physica A **355**, 251 (2005).
[16] S. Okino, S. Akiyama, and H. Hanazaki, Velocity distribution around a sphere descending in a linearly stratified fluid, J. Fluid Mech. **826**, 759 (2017).
[17] X. Pan, K. Kim, C. Lee, and J. I. Choi, Fully decoupled monolithic projection method for natural convection problems, J. Comput. Phys. **334**, 582 (2017).
[18] C. R. Torres, J. Ochoa, J. E. Castillo, and H. Hanazaki, Numerical simulation of flow past a sphere in vertical motion within a stratified fluid, J. Comput. Appl. Math. **103**, 67 (1999).
[19] C. R. Torres, H. Hanazaki, J. Ochoa, J. Castillo, and M. Van Woert, Flow past a sphere moving vertically in a stratified diffusive fluid, J. Fluid Mech. **417**, 211 (2000).
[20] H. Hanazaki, K. Kashimoto, and T. Okamura, Jets generated by a sphere moving vertically in a stratified fluid, J. Fluid Mech. **638**, 173 (2009).
[21] H. Hanazaki, K. Konishi, and T. Okamura, Schmidt-number effects on the flow past a sphere moving vertically in a stratified diffusive fluid, Phys. Fluids **21**, 026602 (2009).
[22] H. Hanazaki, S. Nakamura, and H. Yoshikawa, Numerical simulation of jets generated by a sphere moving vertically in a stratified fluid, J. Fluid Mech. **765**, 424 (2015).
[23] A. N. Sridić-Mitrović, N. A. Mohamed, and H. J. S. Fernando, Gravitational settling of particles through density interfaces, J. Fluid Mech. **381**, 175 (1999).
[24] R. Camassa, C. Falcon, J. Lin, R. M. McLaughlin, and R. Parker, Prolonged residence times for particles settling through stratified miscible fluids in the Stokes regime, Phys. Fluids **21**, 031702 (2009).
[25] R. Camassa, C. Falcon, J. Lin, R. M. McLaughlin, and N. Mykins, A first-principle predictive theory for a sphere falling through sharply stratified fluid at low Reynolds number, J. Fluid Mech. **664**, 436 (2010).
[26] N. Abaid, D. Adalsteinsson, A. Agyapong, and R. M. McLaughlin, An internal splash: Levitation of falling spheres in stratified fluids, Phys. Fluids **16**, 1567 (2004).
[27] F. Blanchette and A. M. Shapiro, Drops settling in sharp stratification with and without Marangoni effects, Phys. Fluids **24**, 042104 (2012).
[28] A. Doostmohammadi, S. Dabiri, and A. M. Ardekani, A numerical study of the dynamics of a particle settling at moderate Reynolds numbers in a linearly stratified fluid, J. Fluid Mech. **750**, 5 (2014).
[29] A. Doostmohammadi and A. M. Ardekani, Suspension of solid particles in a density stratified fluid, Phys. Fluids **27**, 023302 (2015).
[30] A. Doostmohammadi and A. M. Ardekani, Reorientation of elongated particles at density interfaces, Phys. Rev. E **90**, 033013 (2014).

[31] A. Doostmohammadi and A. M. Ardekani, Interaction between a pair of particles settling in a stratified fluid, Phys. Rev. E **88**, 023029 (2013).
[32] M. Bayareh, A. Doostmohammadi, S. Dabiri, and A. M. Ardekani, On the rising motion of a drop in stratified fluids, Phys. Fluids **25**, 103302 (2013).
[33] S. Dabiri, A. Doostmohammadi, M. Bayareh, and A. M. Ardekani, Rising motion of a swarm of drops in a linearly stratified fluid, Int. J. Multiphase Flow **69**, 8 (2015).
[34] R. Camassa, S. Khatri, R. M. McLaughlin, J. C. Prairie, B. L. White, and S. Yu, Retention and entrainment effects: Experiments and theory for porous spheres settling in sharply stratified fluids, Phys. Fluids **25**, 081701 (2013).
[35] M. Panah, F. Blanchette, and S. Khatri, Simulations of a porous particle settling in a density-stratified ambient fluid, Phys. Rev. Fluids **2**, 114303 (2017).
[36] K. Kindler, A. Khalili, and R. Stocker, Diffusion-limited retention of porous particles at density interfaces, Proc. Natl. Acad. Sci. **107**, 22163 (2010).
[37] R. Mehaddi, F. Candelier, and B. Mehlig, Inertial drag on a sphere settling in a stratified fluid, J. Fluid Mech. **855**, 1074 (2018).
[38] J. Zhang, M. J. Mercier, and J. Magnaudet, Core mechanisms of drag enhancement on bodies settling in a stratified fluid, J. Fluid Mech. **875**, 622 (2019).
[39] H. Lee and C. Lee, Drag and torque acting on a sphere rotating in the streamwise direction for the Reynolds number range of $0.02 \leqslant \mathrm{Re} \leqslant 200$, J. Mech. Sci. Technol. **31**, 5285 (2017).
[40] K. Drescher, K. C. Leptos, I. Tuval, T. Ishikawa, T. J. Pedley, and R. E. Goldstein, Dancing Volvox: Hydrodynamic Bound States of Swimming Algae, Phys. Rev. Lett. **102**, 168101 (2009).
[41] C. Maul and S. Kim, Image systems for a stokeslet inside a rigid spherical container, Phys. Fluids **6**, 2221 (1994).
[42] See Supplemental Material at http://link.aps.org/supplemental/10.1103/PhysRevFluids.4.104101 for detailed derivations.
[43] R. Clift, J. R. Grace, and M. E. Weber, *Bubbles, Drops and Particles* (Courier Corporation, North Chelmsford, MA, 2005).
[44] M. C. Gregg, Variations in the intensity of small-scale mixing in the main thermocline, J. Phys. Oceanogr. **7**, 436 (1977).
[45] M. R. Maxey, The gravitational settling of aerosol particles in homogeneous turbulence and random flow fields, J. Fluid Mech. **174**, 441 (1987).
[46] I. Fouxon, Distribution of Particles and Bubbles in Turbulence at a Small Stokes Number, Phys. Rev. Lett. **108**, 134502 (2012).